

1 **Functional characterization of gene regulatory elements and**
2 **neuropsychiatric disease-associated risk loci in iPSCs and iPSC-derived**
3 **neurons**

4

5 **Authors:**

6 Xiaoyu Yang^{1,*}, Ian R. Jones^{1,2,*}, Poshen B. Chen^{3, 4,*}, Han Yang^{1,*}, Xingjie Ren^{1,*}, Lina Zheng⁵,
7 Bin Li³, Yang Eric Li³, Quan Sun^{6,7}, Jia Wen^{6,7}, Cooper Beaman¹, Xiekui Cui¹, Yun Li^{6,7,8}, Wei
8 Wang^{3,5,9}, Ming Hu¹⁰, Bing Ren^{3,11,12,#}, Yin Shen^{1,13,14,#}

9 **Affiliations:**

10 ¹Institute for Human Genetics, University of California, San Francisco, San Francisco, CA, USA.

11 ²Pharmaceutical Sciences and Pharmacogenomics Graduate Program, University of California,
12 San Francisco, San Francisco, CA, USA.

13 ³Department of Cellular and Molecular Medicine, University of California, San Diego, La Jolla, CA,
14 USA.

15 ⁴Genome Institute of Singapore, Agency for Science, Technology and Research (A*STAR),
16 Singapore, Singapore

17 ⁵Bioinformatics and Systems Biology Graduate Program, University of California, San Diego, La
18 Jolla, CA, USA.

19 ⁶Department of Genetics, University of North Carolina, Chapel Hill, NC, USA.

20 ⁷Department of Biostatistics, University of North Carolina, Chapel Hill, NC, USA.

21 ⁸Department of Computer Science, University of North Carolina, Chapel Hill, NC, USA.

22 ⁹Department of Chemistry and Biochemistry, University of California, San Diego, La Jolla, CA,
23 USA.

24 ¹⁰Department of Quantitative Health Sciences, Lerner Research Institute, Cleveland Clinic
25 Foundation, Cleveland, OH, USA.

26 ¹¹Center for Epigenomics, University of California San Diego, School of Medicine, La Jolla, CA,
27 USA.

28 ¹²Ludwig Institute for Cancer Research, La Jolla, CA, USA.

29 ¹³Department of Neurology, University of California, San Francisco, San Francisco, CA, USA.

30 ¹⁴Weill Institute for Neurosciences, University of California, San Francisco, San Francisco, CA, USA
31

32 * These authors contributed equally to the work.

33 # Corresponding authors: Bing Ren biren@health.ucsd.edu and Yin Shen Yin.Shen@ucsf.edu

34 **Abstract**

35 Genome-wide association studies (GWAS) have identified thousands of non-coding variants that
36 contribute to psychiatric disease risks, likely by perturbing *cis*-regulatory elements (CREs).
37 However, our ability to interpret and explore their mechanisms of action is hampered by a lack of
38 annotation of functional CREs (fCREs) in neural cell types. Here, through genome-scale CRISPR
39 screens of 22,000 candidate CREs (cCREs) in human induced pluripotent stem cells (iPSCs)
40 undergoing differentiation to excitatory neurons, we identify 2,847 and 5,540 fCREs essential for
41 iPSC fitness and neuronal differentiation, respectively. These fCREs display dynamic epigenomic
42 features and exhibit increased numbers and genomic spans of chromatin interactions following
43 terminal neuronal differentiation. Furthermore, fCREs essential for neuronal differentiation show
44 significantly greater enrichment of genetic heritability for neurodevelopmental diseases including
45 schizophrenia (SCZ), attention deficit hyperactivity disorder (ADHD), and autism spectrum
46 disorders (ASD) than cCREs. Using high-throughput prime editing screens we experimentally
47 confirm 45 SCZ risk variants that act by affecting the function of fCREs. The extensive and in-
48 depth functional annotation of cCREs in neuronal types therefore provides a crucial resource for
49 interpreting non-coding risk variants of neuropsychiatric disorders.

50 **Main**

51

52 *Cis*-regulatory elements (CREs) play a fundamental role in regulating cell-type-specific gene
53 expression^{1,2}. Great strides have been made in recent years in the annotation of candidate CREs
54 (cCREs) in the human genome through the profiling of their biochemical signatures such as
55 chromatin accessibility, histone modifications, transcription factor (TF) binding, and DNA
56 hypomethylation, etc³⁻⁵, but a shortage of direct functional evidence makes it hard to know if and
57 when the annotated cCREs indeed regulate transcription, emphasizing the urgent need to
58 comprehensively characterize cCREs. The cCREs harbor a disproportionately large number of
59 genetic variants associated with complex human traits and common diseases, supporting the
60 hypothesis that non-coding variants contribute to human diseases and traits largely through the
61 modulation of gene expression^{6,7}. In particular, genome-wide association studies (GWAS) have
62 identified thousands of non-coding genetic variants associated with neuropsychiatric disorders
63 such as schizophrenia⁸ (SCZ), attention deficit hyperactivity disorder⁹ (ADHD), autism spectrum
64 disorder¹⁰ (ASD), and bipolar disorder¹¹ (BD), etc. The genetic heritability of DNA variants
65 associated with neuropsychiatric traits is significantly enriched within cCREs annotated in the
66 glutamatergic neurons compared to non-neuronal cell types¹²⁻¹⁴. However, a dearth of annotated

67 functional CREs (fCREs) in physiologically relevant cell types such as neurons has hindered our
68 ability to identify the disease-causing non-coding variants.

69 To address this knowledge gap, we utilized human induced pluripotent stem cells (iPSCs) and
70 their excitatory neuron differentiation process to perform genome-scale CRISPRi screens
71 combined with multiomic analysis to identify both cCREs and fCREs involved in pluripotency and
72 neuronal differentiation. Through functional characterization of 22,000 cCREs, we identified 2,847
73 fCREs required for iPSC fitness and 5,540 fCREs for neuronal differentiation. We further
74 elucidated the epigenomic features of the fCREs through integrative analysis of matched
75 transcriptome, open chromatin regions, and 3D chromatin interactions. Finally, we demonstrated
76 that fCREs required for neuronal differentiation are strongly enriched with non-coding risk variants
77 linked to schizophrenia, autism, and several other psychiatric disorders, and validated 110 of them
78 through high-throughput prime editing experiments. Our study offers new insights into the
79 regulatory mechanisms of iPSC fitness and neuronal differentiation, with significant implications
80 for understanding the impact of neuropsychiatric disease-associated non-coding variants in
81 disease etiology.

82 **Genome-scale CRISPRi screens for iPSC proliferation and neuronal differentiation**

83 To systematically identify fCREs, we performed pooled CRISPRi screens based on iPSC fitness
84 and excitatory neuron differentiation phenotypes. We introduced a CAG-dCas9-KRAB cassette
85 at the *CLYBL* safe harbor locus in a transgenic iPSC line (i³N-WTC11 iPSCs) (**Extended Data**
86 **Fig. 1a**). The i³N-WTC11 iPSC line contains an integrated, isogenic, and doxycycline-inducible
87 neurogenin-2 (*Ngn2*) cassette at the *AAVS1* safe-harbor locus, enabling rapid induction of
88 excitatory neuron differentiation in a synchronized fashion following doxycycline treatment¹⁵. After
89 CAG-dCas9-KRAB knock-in, we showed that dCas9 expression level in the i³N-dCas9-WTC11
90 iPSC line is comparable to that of a known doxycycline-inducible dCas9-KRAB iPSC line¹⁶
91 (**Extended Data Fig. 1b**), and that CRISPRi exhibits effective knockdown efficiencies in both
92 iPSCs and induced excitatory neurons (**Extended Data Fig. 1c**). Based on these results, we
93 proceeded with genome-scale cCREs screens using this i³N-dCas9-WTC11 iPSC line.

94 For the iPSC fitness screen, we prioritized 16,670 cCREs located within 500 Kbp from the
95 transcription start sites (TSSs) of 1,301 genes previously identified as essential for iPSC
96 fitness^{17,18}. These cCREs overlap with open chromatin regions and H3K27ac occupancy in iPSCs,
97 determined using ATAC-seq and ChIP-seq¹⁹, respectively (**Fig. 1a, Supplementary Table 1a**).
98 For the neuronal differentiation screens, we first selected open chromatin regions identified in

99 iPSC-derived excitatory neurons following a 2-week differentiation, which are located within 500
100 Kbp of 269 genes previously identified as essential for neuronal differentiation or survival using
101 the same differentiation system²⁰. Notably, 170 of the 269 genes (63.2%) were also identified as
102 essential for iPSC fitness in the same study, suggesting that essential genes can be shared
103 between iPSCs and differentiated neurons²⁰. Because these genes were identified from a screen
104 of 2,325 druggable genes, which may not cover all essential genes for neuronal differentiation
105 and fitness, we further expanded our list to include cCREs overlapping with neuronal open
106 chromatin regions and H3K27ac sites²¹ within 500 Kbp of 1,301 iPSC essential genes. Finally,
107 we added 282 neural enhancers annotated by mouse transgenic experiments²². In total, 14,289
108 cCREs were tested in the neuronal differentiation screens (**Fig. 1b, Supplementary Table 1b**).
109 Altogether, we tested 7,126 TSSs and 14,874 distal cCREs in iPSC and neuronal screens, among
110 which 5,000 TSS cCREs and 3,959 distal cCREs (**Methods**) are shared in both screens (**Fig. 1c**),
111 allowing us to assess their context dependent function.

112 For the CRISPRi screens, we employed the dual-gRNA CRISPRi approach as we previously
113 demonstrated more effective dCas9-KRAB-mediated epigenetic silencing using dual-gRNAs
114 targeting a cCRE than using a single gRNA²³. For each cCRE we designed 5 pairs of gRNAs with
115 an average genomic distance of ~300 bp between each pair of gRNAs. In addition, we included
116 8,389 gRNA pairs targeting safe-harbor genomic regions and 1,011 non-targeting gRNA pairs as
117 negative controls^{24,25}. In total, we constructed two lentiviral libraries expressing 88,715 and 66,652
118 pairs of gRNAs for iPSCs and neuronal differentiation screens, respectively (**Extended Data Fig.**
119 **1d-e, Supplementary Table 1c-d**). These dual-guide gRNAs cover 1,120 essential gene loci (+/-
120 500 Kbp for each locus), encompassing a total of ~1 billion base pairs, or nearly one third of the
121 human genome.

122 To identify fCREs required for iPSCs fitness, we infected i³N-dCas9-WTC11 iPSCs at a low
123 multiplicity of infection (MOI) (MOI = 0.5) with the lentiviral library expressing dual-gRNA pairs
124 targeting iPSC cCREs. After five days of puromycin selection (day 0), iPSCs were expanded for
125 another two weeks (day 14). We collected cells at day 0 and 14, amplified the integrated dual-
126 gRNA pairs, and determined copy numbers for each dual-gRNA pair at each time point by deep
127 sequencing (**Fig. 1a**). To identify fCREs essential for neuronal differentiation, we infected i³N-
128 dCas9-WTC11 iPSCs with the lentiviral library expressing dual-gRNA pairs targeting neuronal
129 cCREs (MOI = 0.5). After five days of puromycin selection (day 0), neuronal differentiation was
130 initiated by doxycycline-induced *Ngn2* expression. We collected cells at three time points: day 0
131 (iPSCs), day 3 (pre-differentiated to post-mitotic transition), and day 14 (post-mitotic excitatory

132 neurons). To identify fCREs essential for neuronal differentiation, we compared the copy numbers
133 of dual-gRNA pairs between day 0 and day 3 for pre-differentiation, day 3 and day 14 for post-
134 mitotic differentiation, and day 0 and day 14 for overall neuronal differentiation. By analyzing these
135 three pairwise time point comparisons, we delineate the temporal activity of fCREs during
136 differentiation (**Fig. 1b**). All screens were performed with two biological replicates, with high
137 reproducibility observed between replicates (**Extended Data Fig. 1f-g**).

138 Using the robust ranking aggregation (RRA) method from the MAGECK pipeline²⁶, we identified
139 2,847 fCREs as significantly depleted after 14 passages, indicating their essential role in
140 maintaining iPSC fitness. Similarly, we identified 1,788 fCREs needed for pre-differentiation,
141 3,361 fCREs for post-mitotic differentiation, and 2,150 fCREs for neuronal differentiation (FDR <
142 0.05) (**Fig. 1d, Supplementary Table 2a-d**). As expected, promoter regions of known essential
143 genes were among the top hits in each screen (**Fig. 1d**). Specifically, a recent publication²⁷
144 reported 1,520 essential neuronal genes during *Ngn2*-induced excitatory neuron differentiation.
145 Of these, 968 were included in our design (**Extended Data Fig. 1h**). We observed a strong
146 correlation between our study's gRNA count fold changes for these genes and those of the recent
147 study (**Extended Data Fig. 1i**), with 686 (69.5%) also identified as essential in our study
148 (**Extended Data Fig. 1j**). These observations provide an external validation of the efficacy of our
149 approach for elucidating the functional sequences essential for neuronal differentiation.

150
151 As further independent evidence for the fCREs identified in the CRISPRi screens, we performed
152 CRISPRi experiments to verify the requirements of 6 fCREs in iPSC fitness. Confirming the
153 genome-scale CRISPRi screen results, perturbation of one distal fCRE for *SOX2* (**Fig. 2a**) and
154 two distal fCREs for *MYC* (**Fig. 2b**) led to the downregulation of *SOX2* and *MYC* (**Fig. 2c**) and
155 significantly reduced iPSC survival rate (**Fig. 2d**). We also identified fCREs at *GDF3*, *DUS1L* and
156 *MRPS23* promoters, that potentially regulate *NANOG*, *FASN* and *SRSF1* expression via long-
157 range chromatin interaction (**Extended Data Fig. 2a-c**). *GDF3*, *DUS1L* and *MRPS23*, while
158 expressed in iPSC, were not iPSC essential genes based on the previous small hairpin RNA
159 (shRNA) screen²⁸ and CRISPR knockout screens^{17,18}. In this study, CRISPRi targeting these
160 promoter-proximal fCREs led to down-regulation of *NANOG*, *FASN* and *SRSF1* and decreased
161 cell survival (**Extended Data Fig. 2d-e**). These examples highlighted that our fCREs enable the
162 annotation of regulatory sequences at non-essential gene promoter regions that may work as
163 enhancers to regulate other iPSC fitness genes.

164 We also carried out similar CRISPRi experiments to confirm the role of 4 distal fCREs identified
165 in CRISPRi screens in the neurons. For example, the α -tubulin gene, *TUBA1A*, plays a crucial
166 role in neural development²⁹ and *TUBA1B* (Tubulin Alpha 1b) is an essential gene for neuronal
167 differentiation²⁷. Perturbing fCRE1 near the promoter of *KMT2D* or fCRE2 overlapping an
168 alternative promoter of *TUBA1C* (**Fig. 2e**) led to the downregulation of *TUBA1A*, *TUBA1B*, and
169 *KMT2D* (**Fig. 2f**) and affected neuronal differentiation (**Fig. 2f**). In another example, *EPHB1*
170 encodes a protein belonging to the Ephrin-B family, which is indispensable for neurogenesis³⁰.
171 Two fCREs identified in the intronic region of *EPHB1* (**Extended Data Fig. 2f**) gain chromatin
172 interaction with the *EPHB1* promoter in neurons compared to in iPSCs. Perturbation of *EPHB1*
173 TSS, fCRE1, and fCRE2 affected neuronal differentiation and led to downregulation of *EPHB1*
174 expression (**Extended Data Fig. 2g-h**).

175 As a final piece of evidence supporting the function of the fCREs identified in our CRISPRi screens,
176 we compared the fCREs with previously reported tissue-specific enhancers discovered using
177 transgenic mice²². These experimentally validated fetal brain enhancers (n = 282) are significantly
178 overrepresented in the fCREs found in our neuronal CRISPRi screens (113 out of 282) ($P <$
179 0.01×10^{-3}) but not the iPSC screen (8 out of 85) (**Fig. 2h**). Furthermore, fCREs are more enriched
180 for the neural enhancers identified in transgenic mice (113 out of 282) than the cCREs predicted
181 using ATAC-seq data (1,285 out of 8,031) ($P < 0.01 \times 10^{-3}$) (**Fig. 2i**), supporting the value of fCREs.

182 **fCREs are strongly enriched for active chromatin marks**

183 Our screens identified many novel fCREs in iPSCs fitness (n = 2,516) and neuronal differentiation
184 (n = 4,887), respectively. Specifically, we identified novel fCREs at both TSSs (iPSC: n = 1,264;
185 neuronal screens: n = 2,011) and distal elements (iPSC: n = 1,252; neuronal screens: n = 2,876)
186 (**Fig. 3a, Extended Data Fig. 3a**). Newly identified TSS-proximal fCREs may play a role in cell
187 fitness by directly influencing transcription from these TSSs, or by regulating other nearby genes
188 *in cis*. Indeed 7.5% (n = 121) and 3.5% (n = 98) of the identified TSS fCREs have low expression
189 (RPKM < 1) in iPSC and neuronal differentiation time points respectively, suggesting potential
190 functional roles for those fCREs to act as regulatory sequences for other genes (**Supplementary**
191 **Table 2e**). Strikingly, compared to TSSs of known essential genes, these novel functional TSS
192 proximal and distal fCREs exhibit significantly lower RRA scores for postmitotic and neuronal
193 differentiation processes (**Extended Data Fig. 3b**), demonstrating high sensitivity of dual-gRNA
194 CRISPRi screens in detecting both TSS and distal fCREs, with perturbation of known essential
195 gene TSSs exhibiting larger effect sizes compared to other newly identified fCREs.

196 fCREs are associated with active chromatin marks including chromatin accessibility, H3K27ac
197 and H3K4me3 in iPSCs fCREs, evidenced by a greater enrichment of active chromatin states
198 compared to other cCREs (**Fig. 3b**). Moreover, iPSCs fCREs participated in on average 27.3%
199 more H3K4me3-associated interactions per cCRE, evidenced by Proximity-ligation Assisted ChIP
200 followed by sequencing (PLAC-seq, aka HiChIP) experiments. By contrast, CTCF signal at fCREs
201 decreases by 10.6% despite the number of average CTCF-associated interactions at fCREs
202 slightly increasing by 2.5% (**Fig. 3b**).

203 **Neuronal fCREs display temporal changes in 3D chromatin organization during**
204 **differentiation**

205 By dividing neuronal screens into pre- and post-mitotic differentiation stages, we characterized
206 the temporal dynamics of fCREs during neuronal differentiation. The diversity of fCREs detected
207 throughout neuronal differentiation are highlighted by the low overlap in the fCREs found in the
208 pre-differentiation and post-mitotic screens, with an odds ratio of a cCRE being a fCRE in both
209 screens of 0.38 ($P < 2.2E-16$) (**Fig. 3c, Extended Data Fig. 3c**). To investigate the importance of
210 temporal changes in the 3D epigenome for fCREs identified throughout neuronal differentiation,
211 we conducted RNA-seq, ATAC-seq, and PLAC-seq using antibodies against H3K4me3 and
212 CTCF at differentiation time points corresponding to our screens (**Extended Data Fig. 4a-d, Supple-**
213 **mentary Table 3**). Interestingly, we observed an increase in both numbers and genomic
214 distances of chromatin interactions after differentiation (**Fig. 4a-b**). This finding is consistent with
215 a previous study of dynamic chromatin organization during mESC neural differentiation³¹,
216 suggesting that terminally differentiated neurons could rely on distal gene regulation compared to
217 undifferentiated iPSCs. Additionally, fCREs are significantly associated with chromatin interaction
218 associated with both H3K4me3 and CTCF in the iPSC (Fisher's exact test, $P < 0.01$), post-mitotic
219 differentiation (Fisher's exact test, $P < 0.001$), and neuronal differentiation screens (Fisher's exact
220 test, $P < 0.05$), but are negatively associated in the pre-differentiation screen (Fisher's exact test,
221 $P < 0.001$) (**Fig. 4c, Extended Data Fig. 4e, Supplementary Table 4a-b**). fCREs also participate
222 in more and longer-range chromatin interactions during the differentiation process (**Fig. 4d-f**). For
223 the 17.8% and 24.3% of fCREs that don't engage in H3K4me3- or CTCF-associated chromatin
224 interactions, they tend to reside further away (two-sample t-test, two-tailed, $P < 0.001$) from the
225 nearest TSS than those distal fCREs constantly participating in H3K4me3- or CTCF-associated
226 chromatin interactions throughout differentiation (**Fig. 4g-h**).

227 To elucidate the potential biological roles of fCREs required for neuronal differentiation, we
228 conducted gene ontology (GO) analyses. Both known and newly identified essential genes in

229 iPSC and neuronal screens exhibit an enrichment in fundamental cellular function terms, including
230 mRNA processing, DNA metabolic process, chromatin remodeling and mitochondrial functions
231 (**Extended Data Fig. 4f-g, Supplementary Table 5a-b**). Notably, target genes of neuronal distal
232 fCREs, evidenced by H3K4me3-centered chromatin contacts, are enriched not only in basic
233 cellular functions, but also in such processes as neural nucleus development and neuronal cell
234 recognition (**Fig. 4i, Supplementary Table 5c-d**). Similarly, target genes predicated by CTCF-
235 associated interactions were enriched in processes including synapse organization, neuronal cell
236 recognition, axon guidance, and cell-cell adhesion (**Extended Data Fig. 4h, Supplementary**
237 **Table 5e-f**). Interestingly, these biological processes were not enriched in potential target genes
238 predicted using distance-based annotations by GREAT³² (**Extended Data Fig. 4i,**
239 **Supplementary Table 5g**). We believe that targeting gene annotation by chromatin interaction
240 could better illuminate the role of fCREs in regulating the diverse range of biological pathways
241 during neuronal differentiation.

242 To characterize the dynamic chromatin organization at fCREs during neuronal differentiation, we
243 analyzed the PLAC-seq data and determined 9,445, 13,256, and 18,644 differentially interacting
244 regions (DIRs) centered at promoters marked by constitutive H3K4me3 signals for pre-
245 differentiation (day 0 vs. day 3), post-mitotic (day 3 vs. day 14), and neuronal differentiation (day
246 0 vs. day 14), respectively. We also determined 7,962 DIRs centered at CTCF binding sites for
247 neuronal differentiation (day 0 vs. day 14) (**Extended Data Fig. 5a, Supplementary Table 6**,
248 details in **Methods**). Overall, DIRs are positively correlated with transcriptional changes at their
249 target promoters and distal accessible regions connecting to these promoters display changes in
250 accessibility congruent with transcription from the promoters (**Fig. 5a, Extended Data Fig. 5b**).
251 Furthermore, DIRs centered at promoters are enriched for fCREs identified in the post-mitotic and
252 neuronal differentiation screens but depleted in pre-differentiation fCREs, compared to the rest of
253 the cCREs (**Fig. 5b, Extended Data Fig. 5c, Supplementary Table 4c**). By contrast, DIRs from
254 CTCF binding sites are not enriched for fCREs (**Extended Data Fig. 5d**). We next asked if
255 differentially accessible regions (DARs) are associated with fCREs during differentiation. We
256 analyzed the ATAC-seq data and determined 28,974, 12,246, and 51,101 DARs in pre-
257 differentiation, post-mitotic, and neuronal differentiation, respectively (**Extended Data Fig. 5e,**
258 **Supplementary Table 7**). Notably, fCREs identified from all three screens are enriched for the
259 corresponding DARs (**Fig. 5c, Extended Data Fig. 5f, Supplementary Table 4d**), consistent
260 with their role in regulating gene expression in each differentiation stage.

261 To identify potential TFs that contribute to fCREs function, we determined the TF binding motifs
262 enriched in the promoter-proximal and distal fCREs required for iPSC fitness and neuronal
263 differentiation (**Fig. 5d-e, Supplementary Table 8**). We observed concordant motifs enrichment
264 and TF gene expression in a temporal specific manner along neuronal differentiation. For example,
265 binding motifs for LHX1 and NEUROD1, TFs that are highly expressed in neurons, are enriched
266 at distal fCREs. Interestingly, while FOXO1 binding motif is significantly enriched in fCREs
267 identified in all time points throughout differentiation, the TF itself is only expressed in iPSCs,
268 consistent with its key role in early neuronal fate determination³³. We also found that binding
269 motifs for key neuronal TFs such as MEF2A, MEF2C are significantly enriched at TSS fCREs
270 while NEUROD1 is significantly enriched at distal fCREs, indicating their distinct roles in gene
271 regulation during neuronal differentiation.

272 **Neuropsychiatric risk variants are enriched in neuronal fCREs**

273 We next asked whether fCREs are better suited to partition genetic heritability for complex
274 diseases than cCRE annotated based on biochemical signatures alone. We performed linkage
275 disequilibrium score regression³⁴ (LDSC) using summary statistics from studies of ten
276 neuropsychiatric disorders^{8-11,35-40}. We found that SCZ, ADHD, ASD and post-traumatic stress
277 disorder (PTSD)-associated genetic variants are significantly enriched in neuronal fCREs but not
278 in the non-fitness cCREs (**Fig. 6a**). On the other hand, bipolar disorder (BP) associated variants
279 are enriched in both fCREs and cCREs, while multiple sclerosis (MS) associated variants are
280 exclusively significantly enriched in cCREs, indicating biological processes other than
281 differentiation are associated with these diseases. These results implicate dysregulation of gene
282 expression during neural development as potential contributors of SCZ, ADHD and ASD. By
283 contrast, GWAS variants associated with stroke and Alzheimer's disease (AD) are not enriched
284 in fCREs or cCREs, suggesting cell types other than neurons are more relevant to these diseases.

285 **Functional analysis of SCZ-associated non-coding variants in fCREs**

286 To explore the roles of neural fCREs in the etiology of SCZ, we first tested the function of fCREs
287 overlapping with several SCZ fine-mapped variants⁸ at the *TRAPPC3/LSM10* locus in excitatory
288 neurons (**Fig. 6b**). *TRAPP* is a trafficking protein complex that facilitates vesicle transportation
289 from endoplasmic reticulum to Golgi membrane⁴¹. Mutations in *TRAPP* subunits are linked to a
290 wide range of human diseases⁴², including spondyloepiphyseal dysplasia tarda,
291 hypopigmentation, colorectal cancer, and intellectual disability, etc. For example, *TRAPPC3*⁴³ and
292 *TRAPPC9*⁴⁴ are SCZ risk genes, and *TRAPPC3* and *LSM10* are known neuronal essential genes
293 at this locus²⁷. At this locus, four fCREs are identified by our screens with two of them overlapping

294 with SCZ variants, including rs12033824 and rs12033825 in fCRE1, and rs3754080 and
295 rs10752586 in *TRAPPC3* TSS fCRE2. Notably, the risk allele rs12033824-T could disrupt the
296 binding motif of zinc finger TF ZBTB6, which is highly expressed in neurons and its motif is
297 significantly enriched in neuronal fCREs (**Fig. 6c, Supplementary Table 8**). We found that
298 CRISPRi targeting all four fCREs affect neuronal differentiation (**Fig. 6d, Extended Data Figure**
299 **6**). Perturbing fCRE1 resulted in the downregulation of *LSM10*, while suppressing the promoter
300 of either *TRAPPC3* (fCRE2) or *LSM10* (fCRE4) led to simultaneous down-regulation of both
301 *TRAPPC3* and *LSM10* (**Fig. 6e**). These results illustrate the regulatory complexity of disease-
302 associated non-coding variants and suggest both *TRAPPC3* and *LSM10* are regulated by SCZ
303 risk variants in multiple fCREs.

304 To directly test whether some SCZ non-coding risk variants indeed affect neuronal differentiation,
305 we carried out a high-throughput variant characterization using a newly developed prime editing
306 (PE) screening method⁴⁵. To enable PE screens, we generated a clonal line (i³N-nCas9/RT-
307 WTC11) that has a knock-in of an nCas9 and M-MLV reverse transcriptase (RT) expression
308 cassette at the *CLYBL* locus in i³N-WTC11 iPSC (**Extended Data Fig. 7a-b**). We chose 110 SCZ-
309 associated variants that were discovered from three large SCZ GWAS studies^{8,46,47} (**Methods**)
310 and were located within 58 fCRE regions, and examined their functions in neuronal differentiation
311 in the PE screen. For each SNP, we designed three pairs of prime editing guide RNA and nick
312 gRNA (pegRNAs/ngRNA) to introduce either reference or alternative allele (a total of 656
313 pegRNA/ngRNA pairs). We also included 100 non-targeting negative control pegRNA/ngRNA
314 pairs (**Fig. 7a, Supplementary Table 9a**). We infected i³N-nCas9/RT-WTC11 iPSCs with a lenti-
315 viral library expressing pegRNA/ngRNA pairs at an MOI of 0.3 with two replicates. Infected cells
316 were selected by hygromycin for 5 days before differentiation to excitatory neurons. To investigate
317 the functional difference between the reference and alternative alleles during neuronal
318 differentiation, we calculated pegRNA copy number fold changes in day-14 neurons versus day-
319 0 iPSCs by MAGeCK²⁶. We then obtained the relative fold changes of alternative to reference
320 alleles for each pegRNA/ngRNA at the same nucleotide and identified 45 variants in 29 fCREs as
321 significantly enriched or depleted during neuronal differentiation (FDR < 0.05) (**Fig. 7a-b**,
322 **Supplementary Table 9b-c**). 22, 21 and 19 of the 45 functional SNPs were found within the
323 fCREs characterized from the pre-differentiation screen, post-mitotic deafferentation screen and
324 neuronal differentiation screen, suggesting different roles of functional variants in controlling
325 neural developmental genes in SCZ (**Fig. 7c**). For example, rs1801311 is located in the first exon
326 of *NDUFA6*, which has been implicated in SCZ risk with regulatory functions⁸. The reference allele

327 rs1801311-G, which is also a SCZ risk allele, could disrupt the binding motifs of POLAR2A, TAF1,
328 and YY1, leads to reduced enhancer activity in luciferase reporter assays⁴⁸, and upregulates
329 NAGA expression in the SCZ patient brain⁴⁹. Our study further provides direct evidence that the
330 rs1801311-G allele can confer SCZ risk by reducing neuronal differentiation capacity by 75%
331 (Alt/Ref log₂(fold change) = 2.03) compared to the A allele.

332 Interestingly, we found divergent effects of SCZ risk variants at different stages of neuronal
333 differentiation based on specific differentiation stages. Specifically, risk alleles are more likely to
334 negatively impact post-mitotic differentiation stage (two-sided exact binomial test, $P = 0.049$) than
335 other stages (**Fig. 7d**), consistent with disrupted neurogenesis in SCZ patient derived organoids
336 compared to normal organoids⁵⁰.

337 34 of the 45 functional variants are located in the promoters of 21 genes, and 4 of them,
338 rs2524093, rs2524092, rs2844622 and rs28626310, are located in the promoter of *HLA-C* gene
339 (**Extended Data Fig. 7c**). While *HLA-C* has been recognized for its involvement in immune cell
340 types, recent studies have highlighted the potential involvement of neuronal MHC-I, including
341 *HLA-C*, in neurodevelopment and neurodegenerative diseases^{51,52}. *HLA-C* expression is
342 transiently increased at day 3 after differentiation compared to day 0 and day 14. GTEx^{53,54} eQTL
343 data demonstrated a correlation between three SNPs (rs2524093, rs2524092 and rs2844622)
344 and *HLA-C* expression in brain tissues, with risk alleles associated with increased *HLA-C*
345 expression. It is worth noting that the *HLA-C* promoter interacts with other gene promoters.
346 However, none of these interacting genes are known essential genes or TSS fCREs, suggesting
347 that these four SNPs may exert their functional effects by directly regulating *HLA-C*. Our analyses
348 thus expand the understanding of *HLA-C* beyond its classical immune-related functions and
349 emphasize its potential contributions to neurodevelopmental disorders.

350 Seven functional variants are identified in the locus enriched with multiple SCAN domain-
351 containing TFs, which include rs9393893 in the promoter of *ZKSCAN8*, rs13198809, rs35353359
352 in the promoter of the *ZSCAN31*, and rs1005126, rs4580862, rs4357130, and rs1005127 in the
353 promoter of *ZSCAN12*. All three genes are neuronal genes, with *ZKSCAN8* and *ZSCAN12* in pre-
354 differentiation, and *ZSCAN31* in post-mitotic differentiation (**Fig. 7e**). These three promoters
355 interact with each other, and they also interact with the promoter of another essential gene,
356 *ZSCAN9*, in post-mitotic differentiation and neuronal differentiation. The expression of three
357 *ZSCAN* genes, *ZKSCAN8*, *ZSCAN12* and *ZSCAN9* are upregulated in day 3 and day 14
358 differentiated cells (**Fig. 7e**), consistent with their role in neuronal differentiation. GTEx^{53,54} eQTL

359 data demonstrates that these seven SNPs are associated with the expression of *ZKSCAN8*,
360 *ZSCAN31*, and *ZSCAN9* from different brain regions, highlighting the complexity of this locus with
361 disease-associated variants cooperatively affecting multiple genes through both promoter and
362 enhancer regulations (**Fig. 7f**). In summary, our prime editing screening provides a deeper
363 understanding of the functional SNPs located in fCREs at the base pair resolution. Importantly,
364 our approach offers more detailed functional insights into the role of SCZ SNPs during neuronal
365 differentiation.

366 **Discussion**

367 In this study, we performed genome-scale CRISPRi screens to interrogate the function of 22,000
368 cCREs in iPSC undergoing neuronal differentiation. We identified 2,857 fCREs required for iPSC
369 fitness and 5,540 fCREs required for excitatory neuron differentiation. We delineated differential
370 chromatin features between fCREs and non-essential cCREs, observing increased chromatin
371 accessibility, stronger active H3K27ac and H3K4me3 signals, and a greater quantity of chromatin
372 interactions at fCREs. Furthermore, neuronal fCREs exhibited both increasing chromatin
373 accessibility and interactions over the neuronal differentiation time course. To our knowledge, this
374 study represents the most extensive functional characterization of cCREs in human neurons to
375 date, expanding our knowledge of essential genes^{17,18,20,27} and functional regulatory sequences
376 regulating iPSC fitness and neuron differentiation. The annotation of fCREs provides a great
377 resource of essential DNA elements and genes, and the identified TF binding motifs within
378 promoter-proximal and/or distal fCREs bring new biological insights into iPSC fitness and
379 neuronal differentiation.

380 Individual CRISPRi validations targeting *MYC* and *SOX2* fCREs in iPSCs and *TUBA1A* and
381 *EPHB1* fCREs in neurons not only confirm the fCREs regulatory role in essential gene expression,
382 but also exhibit diverse gene regulatory models including promoter-promoter interactions^{55,56} and
383 co-regulation of multiple target genes⁵⁷. Our assays also confirmed the functionalities of 113 out
384 of 282 developmental brain enhancers previously characterized in transgenic mouse assays²².

385 Previous studies have demonstrated that neuropsychiatric genetic variants are enriched in
386 neuronal cCREs annotated by biochemical signatures¹²⁻¹⁴. In our study, we further narrow-down
387 cCREs to functionally validated fCREs, which offers a better pathway for interpreting the non-
388 coding risk variants associated with neuropsychiatric diseases. In particular, we revealed that
389 fCREs accounts for a high degree of genetic heritability for neurodevelopmental diseases
390 including SCZ, ASD, and ADHD, compared to cCREs, underscoring the value of identifying fCREs

391 during the neuronal differentiation. We further explored SCZ fine-mapped variants using multiple
392 approaches. We first investigated two fCREs covering SCZ variants at the *TRAPPC3/LSM10*
393 locus, and found that perturbations on SCZ risk fCREs affects neuronal differentiation and
394 *TRAPPC3, LSM10* gene expressions. We further performed a prime editing screen targeting 110
395 SCZ genetic variants within neuronal fCREs during neuronal differentiation. 45 causal variants in
396 29 fCREs were identified as essential for the neuronal differentiation process. These functional
397 validations are consistent with GTEx eQTL datasets at the molecular level. Our findings also
398 suggest that SCZ risk genes including *HLA-C, ZKSCAN8, ZSCAN9, ZSCAN12* and *ZSCAN31*
399 may contribute to disease etiology by affecting neuronal development. These results confirmed
400 the significance of functional characterization of neuronal fCREs in understanding the role of
401 neuropsychiatric genetic variants, and identified causal disease risk variants. As the first high-
402 throughput screen at base-pair level for SCZ variants in neurons, our prime-editing screen results
403 provided a paradigm of characterizing endogenous function of GWAS variants in relevant cell
404 types at scale.

405 fCREs in our study are identified based on fitness and differentiation phenotypes. Non-essential
406 cCREs in current screens could be functional in other cell types and biologically processes. Future
407 studies employing other cell types or neuronal phenotypes such as calcium dynamics and
408 synaptic connectivity should offer additional annotation for fCREs and functional disease-
409 associated variants.

410 **Acknowledgements**

411 This work was supported by the National Institutes of Health (NIH) grants UM1HG009402 (to Y.S.
412 and B.R.), and U01DA052713 (to Y.S.). M.H. was partially supported by the NIH grants
413 R35HG011922 and UM1HG011585. J.W. is supported by T32ES007018. This work was made
414 possible in part by NIH grants P30DK063720, and S101S10OD021822-01 to the UCSF
415 Parnassus Flow Cytometry Core. Sequencing was performed at the UCSF CAT, supported by
416 UCSF PBBR, RRP IMIA, and NIH 1S10OD028511-01 grants.

417 **Author contributions**

418 Y.S. and B.R. conceived the study. Y.S. and B.R. supervised the study. X.Y., I.R.J., P.B.C., H.Y.,
419 X.R., C.B. and X.C. performed experiments under the supervision of Y.S. and B.R.. X.Y., I.R.J.,
420 P.B.C., H.Y., L.Z., B.L., Y.E.L., Q.S. and J.W. performed computational analysis under the
421 supervision of Y.S., M.H., Y.L. and B.R.. X.Y., I.R.J., P.B.C., H.Y., M.H., B.R. and Y.S. analyzed

422 and interpreted the data. X.Y., I.R.J, P.B.C., H.Y., B.R., and Y.S. prepared the manuscript with
423 input from all other authors.

424 **Competing interests statement**

425 B.R. is a co-founder and consultant of Arima Genomics Inc. and co-founder of Epigenome
426 Technologies. X.R., H.Y., and Y.S. have filed a patent application related to pooled prime editing
427 screens. The other authors declare no competing interests.

428 **Code availability statement**

429 Data are analyzed using published pipelines with parameters described in the Methods section.
430 No custom code is developed in this study.

431

432 **Data availability statement**

433 PLAC-seq, RNA-seq, and ATAC-seq datasets used in this study are available at the Gene
434 Expression Omnibus under the accession number GSE236705 (reviewer token: cvsbsekirhartud).
435 CRISPRi screens in iPSC and neurons are released by ENCODE portal under the functional
436 characterization experiment series ENCSR499VAT and ENCSR737MRW. Data can be visualized
437 on the WashU Epigenome Browser using the following session bundle ID: 00a68230-389c-11ee-
438 840b-9392e91a6ccc.

439 **Supplementary Tables**

440 Supplementary Table 1 cCRE prioritization and gRNA design in iPSC and neuron CRISPRi
441 screen

442 Supplementary Table 2 MAGeCK analyses for fCREs in iPSC and neuron CRISPRi screens

443 Supplementary Table 3 Epigenetic profiling data processing metrics in neuronal differentiation.

444 Supplementary Table 4 Association analysis for fCREs and chromatin loops.

445 Supplementary Table 5 GO enrichment analysis for essential genes and distal fCRE target genes
446 annotated by H3K4me3- or CTCF-associated interactions

447 Supplementary Table 6 DIRs along neuronal differentiation

448 Supplementary Table 7 DARs along neuronal differentiation

449 Supplementary Table 8 Motif analysis for TSSs and distal fCREs in iPSCs and neurons

450 Supplementary table 9 PegRNA design, counts and functional SCZ SNPs in the prime editing
451 screen

452 Supplementary Table 10 RT-qPCRs primers in individual CRISPRi experiments

453

454 **Figure legends**

455 **Figure 1. Design of CRISPRi screens to identify the fCREs.**

456 **a**, gRNA library design and screening scheme for iPSC self-renewal fCREs. **b**, gRNA library
457 design and screening scheme for neuronal differentiation fCREs. **c**, Overlap of TSSs and distal
458 cCREs assessed in CRISPRi screens in iPSC and neuronal cells. **d**, Genome-wide view of fCREs
459 for iPSC renewal and neuronal differentiation. Top TSS fCREs are labeled. Positive hits are
460 determined by FDR < 0.05.

461 **Figure 2. Independent verification of fCREs required for fitness of iPSC and neuronal
462 differentiation.**

463 **a-b**, Genome browser snapshots of the SOX2 and MYC loci. fCREs from the iPSC, pre-
464 differentiation, post-mitotic, and neuronal screens are colored blue, orange, red, and dark red
465 respectively. Purple boxes indicate the validated fCREs. **c**, CRISPRi effect of perturbing fCREs
466 in iPSC quantified by RT-qPCRs. Boxplots indicate the median and interquartile range. Whiskers
467 indicate the 5th and 95th percentiles. (n = 3, two-tailed two sample t-test). **d**, Survival ratio of
468 fCRE perturbed cells by FACS in iPSC. Data are presented as mean \pm s.d. (n = 3, two-tailed two
469 sample t-test). **e**, Genome browser snapshot of the TUBA1A locus. fCREs from the iPSC, pre-
470 differentiation, post-mitotic, and neuronal screens are colored blue, orange, red, and dark red
471 respectively. Purple boxes indicate the validated fCREs. **f**, CRISPRi effect of perturbing fCREs in
472 neurons quantified by RT-qPCRs. Boxplots indicate the median and interquartile range. Whiskers
473 indicate the 5th and 95th percentiles. (n = 3, two-tailed two sample t-test). **g**, Survival ratio of
474 fCRE perturbed cells by FACS in neuronal differentiation. Data are presented as mean \pm s.d. (n
475 = 3, two-tailed two sample t-test, ns: P > 0.05, *: P < 0.05, **: P < 0.01***: P < 0.001). **h**, Barplot
476 comparing hits percentage for active brain VISTA cCREs in iPSC or neural screens. **i**, Barplot
477 comparing hits percentage for cCREs prioritized by ATAC-seq signal or active brain VISTA
478 cCREs in neural screens. P values are calculated with a two-sided Chi-squared test in (h) and (i).

479 **Figure 3. Genomic and epigenomic features of fCREs.**

480 **a**, Total amount of fCREs recovered from the previously known essential TSSs, novel TSSs, and
481 distal fCREs for each screen. **b**, Violin plots of epigenomic signals between non-fCREs (n =
482 13,823) and fCREs (n = 2,847) from the iPSC screen. (Wilcoxon test, *: P < 0.05, **: P < 0.01, ***:
483 P < 0.001). **c**, Heatmap of odds ratio showing the association between screens. Positive
484 associations (OR > 1, red) are observed between the neuronal screen and either pre-

485 differentiation or post-mitotic differentiation screen. Negative associations (OR < 1, blue) occur
486 between pre-differentiation and post-mitotic screens.

487 **Figure 4. Dynamic 3D chromatin contacts at fCREs during neuronal differentiation.**

488 **a**, Chromatin contacts of H3K4me3- and CTCF- PLAC-seq experiments at each time point along
489 neuronal differentiation. AND interactions are both the interaction bins overlap with anchor bins.
490 XOR interactions are only one of the interaction bins overlap with anchor bins. **b**, Distance
491 distribution of H3K4me3- or CTCF- associated contacts revealing increased 1D distances through
492 differentiation. **c**, Heatmap showing the association between fCREs and chromatin contacts (N
493 are indicated in **Supplementary Table 4a**, Fisher's exact test, *: $P < 0.05$, **: $P < 0.01$, ***: $P <$
494 0.001). **d**, Cumulative distribution function (CDF) plots showing the median interaction distance
495 (dash lines) shift increase through differentiation in H3K4me3- or CTCF- associated chromatin
496 contacts containing fCREs. **e-f**, Numbers of distal fCREs that are involved in H3K4me3- (e) or
497 CTCF- (f) associated chromatin interactions through differentiation. **g-h**, Distance of distal fCREs
498 to their nearest TSS fCRE between fCREs in constant H3K4me3- (g) or CTCF- (h) associated
499 interactions compared to fCREs not participating interactions (midline indicates the median, two-
500 tailed two sample t-test, ***: $P < 0.001$). **i**, Pathway enrichment analysis for fCRE target genes
501 (iPSC proliferation, $n = 385$; pre-differentiation, $n = 229$; post-mitotic differentiation, $n = 715$;
502 neuronal differentiation, $n = 438$) annotated by H3K4me3 associated 3D chromatin interactions
503 (q -value < 0.05).

504 **Figure 5. fCREs undergo chromatin remodeling during neuronal differentiation.**

505 **a**, Heatmap of XOR neuronal DIR containing a distal accessible distal peak. (Left) The observed
506 H3K4me3 PLAC-seq counts over expected counts. (Middle) Summed normalized ATAC-seq
507 signal within distal 5 Kb bin over total ATAC signal across all timepoints. (Right) Summed TMM-
508 RPKM for all genes within distal 5 Kb bin over total expression across all timepoints. **b-c**, Forest
509 plot showing the association of fCREs with (b) DIRs or (c) DARs. Data are shown as odds ratio
510 with 95% confidence interval (N are indicated in **Supplementary Table 4c-d**, Fisher's exact test,
511 *: $P < 0.05$, **: $P < 0.01$, ***: $P < 0.001$). **d-e**, Heatmap showing the top enriched TF motif at TSS
512 (d) or distal (e) fCREs associated with each screen and corresponding TF expression at each
513 time point.

514 **Figure 6. Neuropsychiatric disease-associated risk variants are enriched in neuronal**
515 **fCREs.**

516 **a**, LDSC analysis using annotation of fCREs, non-fitness cCREs or ATAC-seq peaks on
517 neurological disorders. *P*-values are corrected by the Benjamini-Hochberg procedure for multiple
518 tests. FDRs of LDSC coefficients are displayed (*, FDR < 0.05; **, FDR < 0.01; ***, FDR < 0.001).
519 **b**, Genome browser snapshot of the SCZ fine-mapped variants and fCREs near *TRAPPC3*.
520 Purple boxes indicate the validated fCREs. **c**, ZBTB6 motif disrupted by SCZ variant rs12033824
521 within distal fCRE1 at the *TRAPPC3* locus. **d**, Survival ratio of fCRE perturbed cells by FACS in
522 neuronal differentiation. Data are presented as mean \pm s.d. (n = 3, two-tailed two sample t-test).
523 **e**, CRISPRi effect of perturbing fCREs in neurons quantified by RT-qPCRs. Boxplots indicate the
524 median and interquartile range. Whiskers indicate the 5th and 95th percentiles. (n = 3, two-tailed
525 two sample t-test, ns: *P* > 0.05, *: *P* < 0.05, **: *P* < 0.01***: *P* < 0.001).

526 **Figure 7. Functional characterization of SCZ-risk variants within the fCREs.**

527 **a**, (Top) Design of pegRNAs for SCZ-related SNPs. For each variant, three replicates of
528 pegRNA/ngRNA pairs were designed to introduce either the Alt or Ref allele. (Bottom) Workflow
529 of the PE screen. **b**, Volcano plot illustrating the SNPs' impact on neuronal differentiation, with
530 positive or negative effects determined by the relative effect of the Alt versus Ref allele. The
531 dashed line represents the *P* value cutoff determined by non-targeting pegRNAs (FDR < 0.05). n
532 = 2. **c**, Upset plot demonstrating the shared functional SNPs across different types of fCREs. **d**,
533 Bar plot illustrating the effects of risk alleles of functional SNPs on different stages of neuronal
534 differentiation. *P*-values were calculated using the two-sided binomial test. (*: *P* < 0.05) **e**,
535 Genome browser snapshot showing a region with the SCZ risk variants and fCREs enriched with
536 multiple SCAN domain-containing TFs. Red-labeled SNPs indicate positive functional SNPs. **f**,
537 Normalized effect size and *P* values for functional SNPs on regulating target genes based on the
538 GTEx eQTL data in different brain regions. Colors represent normalized effect size and sizes
539 represent *P* values.

540 **Extended Data Figure 1. Summary of the design and results from CRISPRi screens.**

541 **a**, Schematic of genetic knock-in of dCas9-KRAB at the CLYBL safe harbor locus in i³N-WTC11
542 iPSCs. **b**, dCas9 transcription in the i³N-dCas9-WTC11 cell line and i³N-dCas9-WTC11 derived
543 neurons. Transcription levels were compared to Tet-ON-dCas9 WTB (26971820) iPSC treated
544 with doxycycline for 24 hrs by RT-qPCRs. **c**, CRISPRi effect targeting *SDHB* or *NES* promoter
545 quantified by RT-qPCRs in i³N-dCas9-WTC11 and i³N-dCas9-WTC11 derived neurons. Data are
546 shown as mean \pm s.d. (n = 3, two-sided two-sample t-test, ****P* < 0.001). **d**, gRNA library

547 distribution and recovery in the iPSC screen. **e**, gRNA library distribution and recovery in the
548 neuronal screen. **f**, gRNA count reproducibility between biological replicates in the iPSC screen.
549 **g**, gRNA count reproducibility between biological replicates in the neuronal screen. **h**, The chart
550 of cCRE annotation in neuronal screen based on the 2nd study by Tian et al. **i**, Scatterplot showing
551 the correlation of \log_{10} (fold change) and \log_{10} (phenotype score)²⁷ for the neuronal essential genes.
552 Pearson correlation score is labeled (n = 586, $P < 2.2\text{e-}16$). **j**, Count of recovered hits for neuronal
553 essential genes identified by Tian et al.^{20,27}.

554 **Extended Data Figure 2. Individual CRISPRi validation for fCREs in iPSC and neuronal**
555 **differentiation.**

556 **a-c**, Genome browser snapshots of the *NANOG*, *SRSF1* and *FASN* loci. fCREs from the iPSC,
557 pre-differentiation, post-mitotic, and neuronal screens are colored blue, orange, red, and dark red
558 respectively. Purple boxes indicate the validated fCREs. **d**, Survival ratio of fCRE perturbed cells
559 by FACS in iPSC. Data are presented as mean \pm s.d. (n = 3, two-tailed two sample t-test, ns: $P >$
560 0.05, *: $P < 0.05$, **: $P < 0.01$ ***: $P < 0.001$). **e**, CRISPRi effect of perturbing fCREs in iPSC
561 quantified by RT-qPCRs. Boxplots indicate the median and interquartile range. Whiskers indicate
562 the 5th and 95th percentiles. (n = 3, two-tailed two sample t-test). **f**, Genome browser snapshot
563 of the *EPHB1* locus. fCREs from the iPSC, pre-differentiation, post-mitotic, and neuronal screens
564 are colored blue, orange, red, and dark red respectively. Purple boxes indicate the validated
565 fCREs. **g**, Survival ratio of fCRE perturbed cells by FACS in neuronal differentiation. Data are
566 presented as mean \pm s.d. (n = 3, two-tailed two sample t-test, ns: $P > 0.05$, *: $P < 0.05$, **: $P <$
567 0.01***: $P < 0.001$). **h**, CRISPRi effect of perturbing fCREs in neurons quantified by RT-qPCRs.
568 Boxplots indicate the median and interquartile range. Whiskers indicate the 5th and 95th
569 percentiles. (n = 3, two-tailed two sample t-test).

570 **Extended figure 3. Functional annotation of fCREs in iPSC and neuronal differentiation.**

571 **a**, Scatter plot showing the MAGeCK score distribution for fCREs relative to their distance to the
572 nearest TSS. **b**, Distribution of MAGeCK scores for known TSSs, novel TSSs, and distal fCREs
573 for each screen (Wilcoxon test, ns: $P > 0.05$, *: $P < 0.05$, **: $P < 0.01$, ***: $P < 0.001$). **c**, Hits
574 overlap for iPSC and neuron shared cCREs (n = 8,959) tested in the four screens.

575 **Extended Data Figure 4. Epigenomic landscapes of neuronal differentiation and functional**
576 **annotation of essential fCREs.**

577 **a**, PCA plot of RNA-seq. **b**, PCA plot of ATAC-seq. **c**, Heatmap showing the correlation of PLAC-
578 seq datasets by HPRep. **d**, Venn diagram showing the paired-end overlapping of chromatin

579 interactions at different time points in both H3K4me3 and CTCF PLAC-seq. **e**, Heatmap showing
580 the association between fCREs not overlapping anchor bins and XOR chromatin interactions (N
581 are indicated in **Supplementary Table 4b**, Fisher's exact test, *: $P < 0.05$, **: $P < 0.01$, ***:
582 $P < 0.001$). **f**, Pathway enrichment analysis for known essential genes in library design (q-value <
583 0.05, iPSC, n = 1,255; neuron, n = 1,451). **g**, Pathway enrichment analysis for all TSS fCREs
584 corresponding genes in each screen (q-value < 0.05, iPSC proliferation, n = 1,202; pre-
585 differentiation, n = 653; post-mitotic differentiation, n = 1,794; neuronal differentiation, n = 1,172).
586 **h**, Pathway enrichment analysis for distal fCRE target genes annotated by CTCF associated 3D
587 chromatin interactions (q-value < 0.05, iPSC, n = 622; neuron, n = 541). **i**, Biological processes
588 significantly enriched (HyperFdrQ < 0.05) for distal fCREs by GREAT analysis (iPSC proliferation,
589 n = 1,251; pre-differentiation, n = 1,026; post-mitotic differentiation, n = 1,341; neuronal
590 differentiation, n = 910).

591 **Extended Data Figure 5. Dynamics of chromatin organization in neuronal differentiation.**
592 **a**, Scatterplot of differential chromatin interactions, where the x-axis is the 1D genomic distance
593 (unit: Mb) between two interacting 10 Kb bins, and the y-axis is the change of contact frequency
594 measured by $+\/- \text{-log}_{10}(P\text{-value})$. **b**, Boxplots of gene expression (y-axis: measured by
595 $\log_2(\text{RPKM}+1)$) for genes whose promoter overlaps with the differential contacts. In each box, the
596 upper edge, horizontal center line and lower edge represent the 75th percentile, median and 25th
597 percentile, respectively. The upper whiskers represent the 75th percentile $+ 1.5 \times$ the interquartile
598 range (IQR). The lower whiskers represent the minimum values. **c-d**, Forest plot of odds ratio
599 showing the association of distal or TSS fCREs and DIRs identified by H3K4me3 PLAC-seq (c)
600 or CTCF PLAC-seq (d) (N are indicated in **Supplementary Table 4c**, Fisher's exact test, *: $P <$
601 0.05 , **: $P < 0.01$, ***: $P < 0.001$). **e**, Volcano plot of differential accessible regions for the pre-
602 differentiation, post-mitotic, and neuronal differentiation. **f**, Forest plot of odds ratio showing the
603 association of TSS or distal fCREs and DARs (N are indicated in **Supplementary Table 4d**,
604 Fisher's exact test, *: $P < 0.05$, **: $P < 0.01$, ***: $P < 0.001$).

605 **Extended Data Figure 6. Survival ratio of fCRE perturbed cells by flow cytometry.**
606 **a**, iPSC survival after CRISPRi at the *SOX2*, *MYC*, *NANOG*, *SRSF1* and *FASN* fCREs. **b**,
607 Neuronal survival ratio after CRISPRi at the *TUBA1A*, *EPHB1* and *LSM10* fCREs. **c-d**,
608 Representative contour plots depicting FACS gating strategy. Cells were separated from debris
609 of various sizes based on the forward scatter area (FSC-A) and side scatter area (SSC-A). Two
610 singlet gates were applied using the width and height metrics of the side scatter (SSC-H versus

611 SSC-W) and forward scatter (FSC-H versus FSC-W). All singlets are used for survival ratio
612 analysis.

613 **Extended Data Figure 7. HLA-C association with SCZ risk.**

614 **a**, Schematic of genetic knock-in of nCas9/RT at the CLYBL safe harbor locus in i³N-WTC11
615 iPSCs. **b**, nCas9/RT expression in the i³N-nCas9/RT WTC11 cell line (n = 3, two-sided two sample
616 t-test). **c**, Genome browser snapshot showing PE screened SCZ SNPs within a TSS fCRE at the
617 HLA-C promoter. SNPs labeled in red indicate positive functional SNPs.

618

619 **Methods**

620 **Ethics statement**

621 The use of the iPSC line WTC11⁵⁸ was approved by the Human Gamete, Embryo and Stem Cell
622 Research (GESCR) Committee at UCSF.

623 **Cell culture**

624 iPSCs were cultured with mTesR on Matrigel coated plates. Excitatory neurons were derived from
625 isogenic and inducible neurogenin-2 (Ngn2) WTC11 iPSCs (i³N-WTC11) as previously
626 described¹⁵. i³N-WTC11 iPSCs stably expressing dCas9-KRAB or nCas9/RT were generated
627 according to an established method⁵⁹. dCas9-KRAB or nCas9/RT driven by CAG promoter was
628 knocked-in to a safe harbor locus in the intronic region of CLYBL to enable robust transgene
629 expression throughout differentiation. Excitatory neurons were derived in a simplified two-step
630 protocol. In the pre-differentiation stage, i³N-WTC11 iPSCs were cultured with medium containing
631 knockout DMEM/F12 supplemented with 1× N-2, 1× NEAA, 1 µg/ml mouse laminin, 10 ng/ml
632 brain-derived neurotrophic factor (BDNF), 10 ng/ml NT3 and 2 µg/ml doxycycline. ROCK inhibitor
633 (10 µM) was added only for the first day. Medium was changed daily for 3 days. In the post-mitotic
634 differentiation stage, neural progenitor cells were dissociated by Accutase and re-seeded onto
635 Poly-L-ornithine coated plates in medium containing equal parts DMEM/F12 and Neurobasal-A
636 supplemented with 0.5× B-27, 0.5× N-2, 1× NEAA, 0.5× GlutaMax, 1 µg/ml mouse laminin, 10
637 ng/ml BDNF, 10 ng/ml NT3 and 2 µg/ml doxycycline. The doxycycline was omitted in all
638 subsequent medium changes. Half of the medium was changed on day 7 and 2-week excitatory
639 neurons were used for CRISPRi screens.

640 **Design and assembly of the CRISPRi gRNA libraries**

641 iPSC and neuronal essential genes were selected based on previous publications^{17,18,20,27}. 18,220
642 cCREs in iPSCs and 14,736 cCREs in neurons were prioritized as described in the main text for
643 gRNA design. Neural VISTA enhancers were selected if the enhancers are active in neural tube,
644 forebrain, midbrain, hindbrain, dorsal root ganglion and cranial nerve. gRNAs were designed by
645 CRISPR-SE⁶⁰ and selected based on the cutting specificity score greater than 0.3 from
646 GuideScan⁶¹ (v2.0.6). Top 10 ranked gRNA were selected and dual gRNAs were paired by
647 maximizing their distance within each cCREs. 17,743 in iPSC and 14,411 cCREs in neurons were
648 successfully targeted in gRNA design. For negative controls we randomly selected negative
649 gRNAs from previous genome-scale screens^{24,25}. 8,389 safe targeting gRNAs and 1,011 non-
650 targeting gRNAs were included in the screen. The final library contains 88,715 and 66,652 pairs
651 of gRNAs for iPSC and neuron individually. Dual gRNA oligos were synthesized by Agilent and
652 plasmid libraries were assembled in two steps as previously described⁵⁶. In step 1 we amplified
653 the oligo libraries by PCR and purified them with AMPure XP beads. We then performed Gibson
654 assembly reactions to insert gRNA pools into the lenti-Guide-puro backbone (Addgene 52963).
655 The purified product was electroporated into Endura competent cells (Lucigen). We extracted the
656 plasmid pool using the Plasmid Maxi prep kit. In step 2 we digested plasmid pools in step-1 at
657 BsmB-I cutting site between the synthesized paired gRNAs, and ligated with the DNA fragment
658 containing gRNA-scaffold, a linker fragment and the mouse-U6 promoter. The purified DNA
659 ligation product was electroporated into Endura competent cells and plasmid pools were extracted
660 as the final library. Coverage of the library was tested by paired gRNA matches based on
661 amplicons covering the human-U6 promoter and the second gRNA-scaffold. Each step we used
662 a coverage of 1,000 transduced cells per dual-gRNA pair. After library assembly cCREs targeted
663 by low-abundance gRNA pairs were excluded. In total we successfully tested 16,670 cCREs in
664 iPSC and 14,289 cCREs in neuronal CRISPRi screenings.

665 **Pooled CRISPRi screen for iPSC proliferation and neuronal differentiation**

666 Library plasmid pools were packaged into lenti-virus by PsPAX2 (Addgene 12260) and pMD2.G
667 (Addgene 12259) in 293T cells. Lentivirus were concentrated by high-speed centrifuge and titered
668 in iPSC using the survival ratio under antibiotics selection from a serial dilution of lentivirus
669 transduction. In the screens, iPSCs were infected at a low multiplicity of infection (MOI = 0.5) to
670 ensure each infected cell got only one viral particle. 24hrs after infection cells were re-seeded
671 with low density and underwent puromycin selection (0.5 mg/mL, Gibco A1113803) for pooled
672 CRISPRi screen for 5 days. On day 7 after lenti-viral infection we collected cells with a coverage

673 of 1,000 transduced cells per dual-gRNA pair as day-0 library. For the iPSC screen, we kept
674 culturing the cells in regular medium for another 14 days and then collected cells as day-14 library.
675 For the neuronal screen, we started pre-differentiation after antibiotic selection, and collected cells
676 3 days later after pre-differentiation and another 11 days later after post-mitotic differentiation also
677 with a coverage of 1,000 transduced cells per dual-gRNA pair.

678 **Genome wide CRISPRi screen data analysis**

679 The abundance of dual-gRNA pairs from different time points was mapped to the initially designed
680 oligo library sequences using BWA⁶² (v0.7.17). We used MAGeCK²⁶ (v0.5.9.4) to identify fCREs
681 required for cell proliferation. Non-targeting dual-gRNA pairs were provided to generate the null
682 distribution when calculating the *P* values. dual-gRNA pairs were ranked based on the *p*-values,
683 and we used the modified RRA algorithm from MAGeCK to obtain the RRA score for the individual
684 target gene or cCRE. The threshold value for candidate fCREs is the empirical FDR < 0.05 based
685 on the percentage of candidate dual-gRNA pairs identified from negative controls above this
686 threshold, including non-essential genes and safe-target control genomic regions to account for
687 the possible toxicities from the silencing mediated by dCas9-KRAB.

688 **Annotating fCREs**

689 TSS fCREs were defined as fCREs overlapping with a transcriptionally active TSS with an RPKM >
690 1 at any time point of day 0, day 3, or day 14. Distal fCREs were defined as fCREs that do not
691 overlap with any TSSs or overlap with TSSs with RPKM < 1 at all timepoints.

692 **CRIPSRi validation followed by RT-qPCR or FACS**

693 gRNA targeting individual fCREs were synthesized and inserted into modified lenti-Guide puro
694 with GFP tag. iPSCs were infected with lentivirus at MOI ~1. To detect cell survival using FACS,
695 cells were not selected by puromycin but cultured in regular medium for 3 days to ensure all
696 infected cells showed positive GFP expression. We then did FACS analysis to count GFP positive
697 cells on day 0 and day 14, plus day 3 for neurons. Contour plots for gating and representative dot
698 plots are summarized in **Extended Data Fig. 6**. To detect target gene expression by RT-qPCR,
699 cells were selected with puromycin for 5 days. Then we kept culturing iPSC for 14 days before
700 mRNA was extracted. Meanwhile we started neuronal differentiation and mRNA was extracted
701 after 14 days. RT-qPCR primers are listed in **Supplementary Table 10**.

702 **RNA-seq**

703 RNeasy Plus Mini Kit (Qiagen 74134) was used to isolate total RNA and approximately 1 ug of
704 RNA was processed with the TruSeq Stranded mRNA Library Prep Kit (Illumina 20020594) to

705 prepare libraries for paired-end sequencing on Nova-seq 6000. Raw paired-end fastq RNA-seq
706 libraries were filtered for high quality reads and trimmed to 100bp using fastp (v0.22). Next, the
707 libraries were aligned to hg38 using STAR (v2.7.10a) running the standard ENCODE parameters
708 and strand-specific quantification was performed using RSEM (v1.2.28) with the GENCODE 38
709 annotation. TMM-normalized RPKM values for each gene were obtained via the edgeR package.
710 The mean values across all replicates were used for all downstream analyses.

711 **ATAC-seq**

712 ATAC-seq was performed using the Nextera DNA Library Prep Kit (Illumina FC-121-1030). Briefly,
713 each sample received a 1x wash with ice-cold 1x PBS followed by resuspension in ice-cold nuclei
714 extraction buffer (10 mM Tris-HCl pH 7.5, 10 mM NaCl, 3 mM MgCl₂, 0.1% Igepal CA630, and 1x
715 protease inhibitor) for 5 min. 50,000-100,000 cells per reaction were subsequently transferred
716 into 50 μ L 1x buffer TD with 2.5 μ L TDE1 enzyme for 30 min at 37 °C for transposition. DNA was
717 purified with Qiagen MinElute spin columns (Qiagen 28006), PCR amplified, and size-selected
718 with AMPure XP beads. Libraries were then paired-end sequenced on Nova-seq 6000. Reads
719 were trimmed to 50 bp and filtering for high quality reads with fastp (v0.22) were then mapped to
720 hg38 and processed with the ENCODE pipeline (v1.10.0) with default settings. Optimal IDR peaks
721 for each timepoint were used for all downstream analysis. To call DARs, bam and narrowpeak
722 files for each timepoint were supplied to the R package Diffbind⁶³ (v3.4.11) and the DEseq2⁶⁴
723 (v1.38.3) method was used to identify differential peaks, FDR < 0.05 and log₂(fold change) < 0.5,
724 from a union peak set.

725 **PLAC-seq**

726 PLAC-seq libraries were generated using the Arima-HiC⁺ kit (P/N A101020) according to the
727 manufacturer's protocol. Briefly, 3-5 million cells or approximately 15 ug of DNA crosslinked with
728 2% PFA (Fisher Scientific F79-500) were used as input per reaction. Following restriction
729 digestion, biotinylation, and proximal ligation, the chromatin was sheared with a Covaris S220
730 sonicator to fragments between 300 and 1,000 bp and subsequently and immunoprecipitated with
731 anti-H3K4me3 antibody (Millipore 04-745) or anti-CTCF antibody (Active Motif 91285).
732 Immunoprecipitated chromatin was then indexed with the Accel-NGS 2S Plus DNA Library Kit
733 (Swift Biosciences 21024) and amplified with KAPA Library Amplification Kit (Roche KK2620),
734 before paired-end next generation sequencing.

735 **PLAC-seq data processing**

736 We used MAPS⁶⁵ (v1.1.0) to call significant interactions using default parameters at 5 Kb
737 resolution for both H3K4me3 and CTCF associated PLAC-seq libraries. Briefly, BWA (v0.7.17)
738 was used to map the raw reads to hg38. After removing low quality and non-mapped reads,
739 anchor regions were defined by using the MACS2 (v2.2.4) callpeak command with the following
740 options “--broad --nolambda --broad-cutoff 0.01” on read pairs with an interaction distance < 1 Kb
741 normalized by sequencing depth for each timepoint. A final anchor set was generated by taking
742 the union of all timepoints for both H3K4me3 and CTCF conditions. Next read pairs were defined
743 as AND, XOR, or NOT interactions based on whether both, one, or neither of the contact bins
744 overlapped with union anchors. Only intrachromosomal AND and XOR pairs between 10 Kb ~ 2
745 Mb were retained for downstream analysis. HPrep⁶⁶ (v1.0) was used to confirm reproducibility
746 between replicates before merging them. Significant interactions were called using approximately
747 41 ~ 43 million usable reads per time point. Significant interactions were called as previously
748 described⁶⁵.

749 **Contact Probability**

750 We calculated contact probability similarly as previously described³¹. Briefly, we first determined
751 the total number of paired PLAC-seq reads between 10 Kb and 2,560 Kb. Next, we obtained the
752 contact probability as the sum of observed paired counts within a log2 distance divided by the
753 total. Finally, we plotted the best fitting line between distances using a loess curve.

754 **Epigenomic Signal Comparison**

755 H3K27ac (ENCFF573DHK), H3K4me3 (ENCFF577IZN) and CTCF (ENCFF974CGC) ChIP-seq
756 signals were obtained from ENCODE, while the ATAC-seq and PLAC-seq contacts were
757 generated in this study. Next, the bigWigAverageOverBed (v302.1) command was used to obtain
758 the signal overlapping with the 16,583 cCREs in the iPSC screen for the H3K27ac, H3K4me3,
759 CTCF and ATAC signal. The bedtools (v2.29.0) pairToBed command was used to count the
760 number of interactions per cCRE. Finally, the Wilcoxon test measured significant differences
761 between the mean values.

762 **Target genes annotation for distal fCREs and GO enrichment analysis**

763 Target genes of distal fCREs were annotated by PLAC-seq datasets. First, anchor bins are
764 annotated by TSS overlap. Then distal fCREs were intersected with both anchor bins and target
765 bins to get all potential target genes (**Supplementary Table 5**). We further filtered target genes
766 by RPKM > 1 in day 0 for iPSCs, in day 3 or day 14 for neurons, and excluded genes that have

767 been validated as non-essential in our screens. GO enrichment analysis was performed using
768 clusterProfiler⁶⁷ (v3.18.1). Known essential genes, new essential genes and distal fCRE target
769 genes annotated by H3K4me3- and CTCF-associated PLAC-seq were used as input compared
770 to a genome wide background gene list. Enriched GO terms in the “GO Biological Process”
771 ontology with q-value < 0.05 were reported (**Supplementary Table 5**).

772 **Identification of DIRs**

773 We applied edgeR⁶⁸ (v3.32.1) to identify DIRs as described in our previous study⁶⁹. We used the
774 comparison between H3K4me3 PLAC-seq data at day 0 and day 3 as an illustrative example to
775 demonstrate our data analysis procedure. Briefly, we first used MACS2⁷⁰ (v2.2.4) to call H3K4me3
776 ChIP-seq peaks, described above, at day 0 and day 3, and defined differential H3K4me3 ChIP-
777 seq peaks between two time point if (1) FDR < 5% and (2) $\log_2(\text{fold change}) > 0.5$. Next, we
778 selected 5 Kb bin pairs anchored at the non-differential H3K4me3 ChIP-seq peaks for the
779 differential chromatin interaction analysis, to ensure that the dynamics of chromatin contact
780 frequency is not biased by the dynamics of protein binding intensity. We started from 5 Kb bin
781 pairs with 1D genomic distance 5 Kb ~ 2 Mb, and contained ≥ 20 reads in at least one replicate.
782 We then stratified all selected 5 Kb bin pairs into 1D genomic distance groups from 5 Kb to 150
783 Kb. For the remaining 5 Kb bin pairs with 1D genomic distance > 150 Kb, we stratified them into
784 groups such that each group contains the same number of 5 Kb bin pairs as that in the group of
785 5 Kb bin pairs with 1D genomic distance 150 Kb. For 5 Kb bin pairs in each group, we applied
786 edgeR to evaluate the statistical significance of the difference in chromatin contact frequency. We
787 defined a 5 Kb bin pair as a DIR if FDR < 0.01 and $\log_2(\text{fold change}) > 1$. To visualize the identified
788 DIRs, we plotted 1D genomic distance vs. the magnitude of change of chromatin contact
789 frequency, defined as the signed $-\log_{10}(P\text{-value})$. We applied the same approach to identify DIR
790 for H3K4me3 PLAC-seq data between day 0 and day 14, day 3 and day 14, and CTCF PLAC-
791 seq data between day 0 and day 14.

792 **Heatmap**

793 Significant interactions specific to one time point or interactions labeled as DIRs between two
794 timepoints were prioritized. Next, we further filtered for only XOR interactions. The contact
795 frequency was determined by the observed count between bin pairs over the expected count
796 generated by MAPs. Next the ratio of ATAC-seq signal was calculated in the following manner.
797 First, a union peak set of all time points was made by concatenating all IDR peaks and
798 subsequently merging them with the bedtools merge command. Next, the ATAC-seq signal for
799 each time point was obtained by using the bigWigAverageOverBed from sequencing depth

800 normalized bigwig files. The signal was further quantile-normalized with the normalize.quantiles()
801 function in R (v4.2.2). Lastly, if multiple signals occurred within the same bin, they were summed.
802 The heatmap displays the percentage of the individual time point over the total signal summed
803 across all samples. Similarly, transcription of all genes within the anchor bin was displayed as the
804 individual TMM-RPKM over the total expression summed across all samples.

805 **Motif analysis**

806 Motif enrichment analysis using HOMER⁷¹ (v4.11.1) running the default settings. fCREs from
807 iPSC screen and pooled neural screens were used as input. ATAC-seq peaks in iPSC and day
808 14 neurons were used as background. The hypergeometric distribution was used for motif scoring.
809 Significance and expression values for top detected motif and its corresponding TFs are reported.
810 Cell type specific or shared motifs are categories based on motif enrichment lists, with the cell
811 type specific TF expression considered. A full list of motifs is reported in **Supplementary Table**
812 **8**.

813 **LDSC analysis**

814 Three sets of genomic regions were used for LDSC (v1.0.1) analyses, including 1) fCREs from
815 CRISPRi screens; 2) non-fitness cCREs from CRISPRi screens. 3) the chromatin accessible
816 regions were identified from ATAC-seq for day 0 iPSC, day 3 and day 14 neurons. To enable
817 comparison to GWAS of human phenotypes, we used liftOver with default setting “-
818 minMatch=0.95” to convert accessible elements from hg38 to hg19 genomic coordinates. GWAS
819 summary statistics were downloaded for quantitative traits related to neurological disease
820 including SCZ⁸, ADHD⁹, ASD¹⁰, BD¹¹, PTSD³⁵, MS³⁶, neuroticism³⁷, stroke³⁸, alcohol usage⁴⁰ and
821 AD³⁹. We prepared summary statistics to the standard format for LD score regression³⁴. For the
822 analysis using fCREs, non-fitness cCREs, and ATAC-seq peaks as annotations, we take the
823 superset of chromatin accessible regions in day 0 iPSC, day 3 and day 14 neurons as the
824 background control. For each trait, LD score regression was performed to estimate the enrichment
825 coefficient of each annotation jointly with the background controls.

826 **Design and assembly of the prime editing screening library**

827 SCZ GWAS SNPs were initially selected if supported by at least two studies from four SCZ
828 studies^{8,46,47,72}. A significance threshold of $P < 5e-8$ was applied to the three GWAS studies^{8,46,47},
829 while for DeepGWAS⁷², a posterior probability greater than 0.5 was utilized. SNPs in linkage
830 disequilibrium with these initial variants ($r^2 > 0.6$) were also incorporated from the TOP-LD
831 database⁷³, focusing on the EUR population, resulting in a comprehensive collection of 25,999

832 SNPs. Subsequently, we identified 110 variants situated within neuronal differentiation fCREs.
833 Prime editing was performed using PE3 system⁷⁴. For each SNP, pegRNAs were designed to edit
834 the variants into either reference or alternative alleles using the default parameters of the
835 PrimeDesign software⁷⁵ (v0.2). To increase transcription efficiency from the U6 promoter, a
836 guanine nucleotide was added to the 5' end of all pegRNAs/ngRNAs with leading nucleotides
837 other than G. We eliminated pegRNA/ngRNA pairs containing BsmBI sites (GAGACG, CGTCTC)
838 or a TTTTT sequence in the pegRNA spacer, ngRNA spacer, or pegRNA extension. When
839 multiple pairs were available for the same locus, pegRNA/ngRNA pairs were selected to maximize
840 specificity, efficiency, and the distance between ngRNA and pegRNA, while minimizing the editing
841 distance between pegRNA and the target. For each allele, we attempted to design three unique
842 pairs of pegRNAs. For non-targeting pegRNA/ngRNA pairs, the pegRNA spacer, ngRNA spacer,
843 and pegRNA extension sequences were selected from the ENCODE non-targeting sgRNA
844 reference dataset (<https://www.encodeproject.org/files/ENCFF058BPG/>). The final pegRNA pool
845 comprised 656 experimental pegRNAs and 100 negative control pegRNAs that do not target the
846 human genome. To link these component sequences, we used the following template: 5'-
847 CTTGGAGAAAAGCCTTGT[ngRNA-spacer]GTTTAGAGACG[5nt-random-
848 sequence]CGTCTCACACC[pegRNA-
849 spacer]GTTTAGAGCTAGAAATAGCAAGTTAAATAAGGCTAGTCCGTTATCAACTGAAAA
850 AGTGGCACCGAGTCGGTGC[pegRNA-extension]CCTAACACCCGCGGGTTC-3'.
851 Library oligos for the prime editing screen were synthesized by Twist Bioscience and amplified
852 using the NEBNext High-Fidelity 2x PCR Master Mix (NEB M0541L) with the forward primer
853 GTGTTTGAGACTATAATATCCCTTGGAGAAAAGCCTTGT and the reverse primer
854 CTAGTTGGTTAACGCGTAACTAGATAGAACCGCGGTGTTAGG. To amplify paired
855 PegRNA/ngRNA library oligos, we employed emulsion PCR (ePCR) to reduce recombination of
856 similar amplicons during PCR. In brief, we performed 96 20 μ l ePCR reactions using 0.01 fmol of
857 pooled oligos with NEBNext High-Fidelity 2x PCR Master Mix. Each 20 μ l PCR mix was combined
858 with 40 μ l of an oil-surfactant mixture (containing 4.5% Span 80 (v/v), 0.4% Tween 80 (v/v), and
859 0.05% Triton X-100 (v/v) in mineral oil). This mixture was vortexed at maximum speed for 5 min,
860 briefly centrifuged, and placed into the PCR machine for amplification. The thermocycler settings
861 were as follows: 98 °C for 30 s, followed by 26 cycles (98 °C for 10 s, 60 °C for 20 s, 72 °C for 30
862 s), then 72 °C for 5 min, and finally a 4 °C hold. The ramp rate for each step was 2°C/s. After
863 PCR, individual reactions were combined and purified using the QIAQuick PCR Purification Kit
864 (Qiagen 28104). Purified PCR products were then treated with Exonuclease I (NEB M0568L) and
865 purified using 1x AMPure XP beads (Beckman Coulter A63881). The isolated ePCR products

866 were inserted into a BsmBI-digested lentiV2-mU6-evoPREQ1 vector via Gibson assembly (NEB
867 E2621L). The assembled products were electroporated into Endura electrocompetent cells
868 (Biosearch Technologies 60242), and approximately 4,000 independent bacterial colonies were
869 cultured for each library. The resulting plasmid DNA was linearized by BsmBI digestion, gel-
870 purified, and ligated using T4 ligase (NEB M0202M) to a DNA fragment containing an sgRNA
871 scaffold and the human U6 promoter. The resulting library was electroporated into Endura
872 electrocompetent cells and cultured as described above. Finally, the plasmid library was extracted
873 using the Qiagen EndoFree Plasmid Mega Kit (Qiagen 12381).

874 **Prime editing screen data analysis**

875 Sequencing libraries underwent an initial step of trimming 5 bp random sequences from both
876 read-1 and read-2. Subsequently, low-quality reads were filtered out using fastp (v0.22) before
877 formal mapping. Read counts were calculated based on specific criteria for each pegRNA/ngRNA
878 pair, which included: (1) read-1 exactly matches the sequence containing a 20-21 nt ngRNA
879 spacer and 5 bp flanking sequences, and (2) read-2 exactly matches the reverse complementary
880 sequence containing the complete pegRNA extension and 5 bp flanking sequences. For all
881 samples, oligo counts were inputted into MAGeCK²⁶ (v0.5.9.4) to determine the fold changes of
882 each oligo by comparing the day 14 data to the day 0 data with the normalization with control non-
883 targeting. Subsequently, the log₂(fold change) of each pegRNA was used to calculate the relative
884 fold change for SNPs (alternative to reference). In order to create the control non-targeting SNP,
885 we randomly grouped two pegRNA/ngRNA designs as reference and alternative for the non-
886 targeting SNPs, and three pairs were grouped together for a single non-targeting SNPs design.
887 To calculate the fold change and *P*-value of the SNPs, we combined all experimental SNPs and
888 non-targeting SNPs and utilized the MAGeCK (v0.5.9.4) RRA method. To minimize false positive
889 results and maintain an empirical FDR below 5%, we selected a *P*-value cutoff corresponding to
890 the minimal *P*-values obtained from the non-targeting SNPs.

891 **Statistics and reproducibility**

892 Statistical methods used are indicated in the figure legends or Methods sections. No statistical
893 method was used to predetermine sample size, and no data were excluded from analysis. The
894 experiments were not randomized. The Investigators were not blinded to allocation during
895 experiments and outcome assessment.

896

897 **Reference**

- 898 1 Roadmap Epigenomics, C. *et al.* Integrative analysis of 111 reference human epigenomes.
899 2 *Nature* **518**, 317-330, doi:10.1038/nature14248 (2015).
- 900 2 Consortium, E. P. *et al.* Expanded encyclopaedias of DNA elements in the human and
901 mouse genomes. *Nature* **583**, 699-710, doi:10.1038/s41586-020-2493-4 (2020).
- 902 3 Heintzman, N. D. *et al.* Distinct and predictive chromatin signatures of transcriptional
903 promoters and enhancers in the human genome. *Nat Genet* **39**, 311-318,
904 doi:10.1038/ng1966 (2007).
- 905 4 Boyle, A. P. *et al.* High-resolution mapping and characterization of open chromatin across
906 the genome. *Cell* **132**, 311-322, doi:10.1016/j.cell.2007.12.014 (2008).
- 907 5 Ziller, M. J. *et al.* Charting a dynamic DNA methylation landscape of the human genome.
908 *Nature* **500**, 477-481, doi:10.1038/nature12433 (2013).
- 909 6 Maurano, M. T. *et al.* Systematic localization of common disease-associated variation in
910 regulatory DNA. *Science* **337**, 1190-1195, doi:10.1126/science.1222794 (2012).
- 911 7 Edwards, S. L., Beesley, J., French, J. D. & Dunning, A. M. Beyond GWASs: illuminating
912 the dark road from association to function. *Am J Hum Genet* **93**, 779-797,
913 doi:10.1016/j.ajhg.2013.10.012 (2013).
- 914 8 Schizophrenia Working Group of the Psychiatric Genomics, C. Biological insights from
915 108 schizophrenia-associated genetic loci. *Nature* **511**, 421-427,
916 doi:10.1038/nature13595 (2014).
- 917 9 Demontis, D. *et al.* Discovery of the first genome-wide significant risk loci for attention
918 deficit/hyperactivity disorder. *Nat Genet* **51**, 63-75, doi:10.1038/s41588-018-0269-7
919 (2019).
- 920 10 Grove, J. *et al.* Identification of common genetic risk variants for autism spectrum disorder.
921 *Nat Genet* **51**, 431-444, doi:10.1038/s41588-019-0344-8 (2019).
- 922 11 Hou, L. *et al.* Genome-wide association study of 40,000 individuals identifies two novel
923 loci associated with bipolar disorder. *Hum Mol Genet* **25**, 3383-3394,
924 doi:10.1093/hmg/ddw181 (2016).
- 925 12 Skene, N. G. *et al.* Genetic identification of brain cell types underlying schizophrenia. *Nat
926 Genet* **50**, 825-833, doi:10.1038/s41588-018-0129-5 (2018).
- 927 13 Li, M. *et al.* Integrative functional genomic analysis of human brain development and
928 neuropsychiatric risks. *Science* **362**, doi:10.1126/science.aat7615 (2018).
- 929 14 Li, Y. E. *et al.* A comparative atlas of single-cell chromatin accessibility in the human brain.
930 *bioRxiv*, 2022.2011.2009.515833 (2022).
- 931 15 Wang, C. *et al.* Scalable Production of iPSC-Derived Human Neurons to Identify Tau-
932 Lowering Compounds by High-Content Screening. *Stem Cell Reports* **9**, 1221-1233,
933 doi:10.1016/j.stemcr.2017.08.019 (2017).
- 934 16 Mandegar, M. A. *et al.* CRISPR Interference Efficiently Induces Specific and Reversible
935 Gene Silencing in Human iPSCs. *Cell Stem Cell* **18**, 541-553,
936 doi:10.1016/j.stem.2016.01.022 (2016).
- 937 17 Ihry, R. J. *et al.* Genome-Scale CRISPR Screens Identify Human Pluripotency-Specific
938 Genes. *Cell Rep* **27**, 616-630 e616, doi:10.1016/j.celrep.2019.03.043 (2019).
- 939 18 Mair, B. *et al.* Essential Gene Profiles for Human Pluripotent Stem Cells Identify
940 Uncharacterized Genes and Substrate Dependencies. *Cell Rep* **27**, 599-615 e512,
941 doi:10.1016/j.celrep.2019.02.041 (2019).
- 942 19 Ren, X. *et al.* Parallel characterization of cis-regulatory elements for multiple genes using
943 CRISPRpath. *Sci Adv* **7**, eabi4360, doi:10.1126/sciadv.abi4360 (2021).
- 944 20 Tian, R. *et al.* CRISPR Interference-Based Platform for Multimodal Genetic Screens in
945 Human iPSC-Derived Neurons. *Neuron* **104**, 239-255 e212,
946 doi:10.1016/j.neuron.2019.07.014 (2019).

- 947 21 Song, M. *et al.* Mapping cis-regulatory chromatin contacts in neural cells links
948 neuropsychiatric disorder risk variants to target genes. *Nat Genet* **51**, 1252-1262,
949 doi:10.1038/s41588-019-0472-1 (2019).
- 950 22 Visel, A., Minovitsky, S., Dubchak, I. & Pennacchio, L. A. VISTA Enhancer Browser--a
951 database of tissue-specific human enhancers. *Nucleic Acids Res* **35**, D88-92,
952 doi:10.1093/nar/gkl822 (2007).
- 953 23 Chen, P. B. *et al.* Systematic discovery and functional dissection of enhancers needed for
954 cancer cell fitness and proliferation. *Cell Rep* **41**, 111630,
955 doi:10.1016/j.celrep.2022.111630 (2022).
- 956 24 Morgens, D. W. *et al.* Genome-scale measurement of off-target activity using Cas9 toxicity
957 in high-throughput screens. *Nat Commun* **8**, 15178, doi:10.1038/ncomms15178 (2017).
- 958 25 Reilly, S. K. *et al.* Direct characterization of cis-regulatory elements and functional
959 dissection of complex genetic associations using HCR-FlowFISH. *Nat Genet* **53**, 1166-
960 1176, doi:10.1038/s41588-021-00900-4 (2021).
- 961 26 Li, W. *et al.* MAGeCK enables robust identification of essential genes from genome-scale
962 CRISPR/Cas9 knockout screens. *Genome Biol* **15**, 554, doi:10.1186/s13059-014-0554-4
963 (2014).
- 964 27 Tian, R. *et al.* Genome-wide CRISPRi/a screens in human neurons link lysosomal failure
965 to ferroptosis. *Nat Neurosci* **24**, 1020-1034, doi:10.1038/s41593-021-00862-0 (2021).
- 966 28 Kagey, M. H. *et al.* Mediator and cohesin connect gene expression and chromatin
967 architecture. *Nature* **467**, 430-435, doi:10.1038/nature09380 (2010).
- 968 29 Keays, D. A. *et al.* Mutations in alpha-tubulin cause abnormal neuronal migration in mice
969 and lissencephaly in humans. *Cell* **128**, 45-57, doi:10.1016/j.cell.2006.12.017 (2007).
- 970 30 Chumley, M. J., Catchpole, T., Silvany, R. E., Kernie, S. G. & Henkemeyer, M. EphB
971 receptors regulate stem/progenitor cell proliferation, migration, and polarity during
972 hippocampal neurogenesis. *J Neurosci* **27**, 13481-13490,
973 doi:10.1523/JNEUROSCI.4158-07.2007 (2007).
- 974 31 Bonev, B. *et al.* Multiscale 3D Genome Rewiring during Mouse Neural Development. *Cell*
975 **171**, 557-572 e524, doi:10.1016/j.cell.2017.09.043 (2017).
- 976 32 McLean, C. Y. *et al.* GREAT improves functional interpretation of cis-regulatory regions.
977 *Nat Biotechnol* **28**, 495-501, doi:10.1038/nbt.1630 (2010).
- 978 33 Paik, J. H. *et al.* FoxOs cooperatively regulate diverse pathways governing neural stem
979 cell homeostasis. *Cell Stem Cell* **5**, 540-553, doi:10.1016/j.stem.2009.09.013 (2009).
- 980 34 Bulik-Sullivan, B. K. *et al.* LD Score regression distinguishes confounding from
981 polygenicity in genome-wide association studies. *Nat Genet* **47**, 291-295,
982 doi:10.1038/ng.3211 (2015).
- 983 35 Logue, M. W. *et al.* The Psychiatric Genomics Consortium Posttraumatic Stress Disorder
984 Workgroup: Posttraumatic Stress Disorder Enters the Age of Large-Scale Genomic
985 Collaboration. *Neuropsychopharmacology* **40**, 2287-2297, doi:10.1038/npp.2015.118
986 (2015).
- 987 36 International Multiple Sclerosis Genetics, C. Multiple sclerosis genomic map implicates
988 peripheral immune cells and microglia in susceptibility. *Science* **365**,
989 doi:10.1126/science.aav7188 (2019).
- 990 37 Luciano, M. *et al.* Association analysis in over 329,000 individuals identifies 116
991 independent variants influencing neuroticism. *Nat Genet* **50**, 6-11, doi:10.1038/s41588-
992 017-0013-8 (2018).
- 993 38 Malik, R. *et al.* Multiancestry genome-wide association study of 520,000 subjects identifies
994 32 loci associated with stroke and stroke subtypes. *Nat Genet* **50**, 524-537,
995 doi:10.1038/s41588-018-0058-3 (2018).

- 996 39 Jansen, I. E. *et al.* Genome-wide meta-analysis identifies new loci and functional pathways
997 influencing Alzheimer's disease risk. *Nat Genet* **51**, 404-413, doi:10.1038/s41588-018-
998 0311-9 (2019).
- 999 40 Schumann, G. *et al.* KLB is associated with alcohol drinking, and its gene product beta-
1000 Klotho is necessary for FGF21 regulation of alcohol preference. *Proc Natl Acad Sci U S A*
1001 **113**, 14372-14377, doi:10.1073/pnas.1611243113 (2016).
- 1002 41 Sacher, M. *et al.* TRAPP, a highly conserved novel complex on the cis-Golgi that mediates
1003 vesicle docking and fusion. *EMBO J* **17**, 2494-2503, doi:10.1093/emboj/17.9.2494 (1998).
- 1004 42 Brunet, S. & Sacher, M. In sickness and in health: the role of TRAPP and associated
1005 proteins in disease. *Traffic* **15**, 803-818, doi:10.1111/tra.12183 (2014).
- 1006 43 Aberg, K. A. *et al.* A comprehensive family-based replication study of schizophrenia genes.
1007 *JAMA Psychiatry* **70**, 573-581, doi:10.1001/jamapsychiatry.2013.288 (2013).
- 1008 44 McCarthy, S. E. *et al.* De novo mutations in schizophrenia implicate chromatin remodeling
1009 and support a genetic overlap with autism and intellectual disability. *Mol Psychiatry* **19**,
1010 652-658, doi:10.1038/mp.2014.29 (2014).
- 1011 45 Ren, X. *et al.* High throughput PRIME editing screens identify functional DNA variants in
1012 the human genome. *bioRxiv*, 2023.2007. 2012.548736 (2023).
- 1013 46 Pardinas, A. F. *et al.* Common schizophrenia alleles are enriched in mutation-intolerant
1014 genes and in regions under strong background selection. *Nat Genet* **50**, 381-389,
1015 doi:10.1038/s41588-018-0059-2 (2018).
- 1016 47 Trubetskoy, V. *et al.* Mapping genomic loci implicates genes and synaptic biology in
1017 schizophrenia. *Nature* **604**, 502-508, doi:10.1038/s41586-022-04434-5 (2022).
- 1018 48 Huo, Y., Li, S., Liu, J., Li, X. & Luo, X. J. Functional genomics reveal gene regulatory
1019 mechanisms underlying schizophrenia risk. *Nat Commun* **10**, 670, doi:10.1038/s41467-
1020 019-08666-4 (2019).
- 1021 49 Li, Y. *et al.* A missense variant in NDUFA6 confers schizophrenia risk by affecting YY1
1022 binding and NAGA expression. *Mol Psychiatry* **26**, 6896-6911, doi:10.1038/s41380-021-
1023 01125-x (2021).
- 1024 50 Notaras, M. *et al.* Schizophrenia is defined by cell-specific neuropathology and multiple
1025 neurodevelopmental mechanisms in patient-derived cerebral organoids. *Mol Psychiatry*
1026 **27**, 1416-1434, doi:10.1038/s41380-021-01316-6 (2022).
- 1027 51 Shatz, C. J. MHC class I: an unexpected role in neuronal plasticity. *Neuron* **64**, 40-45,
1028 doi:10.1016/j.neuron.2009.09.044 (2009).
- 1029 52 Zalocusky, K. A. *et al.* Neuronal ApoE upregulates MHC-I expression to drive selective
1030 neurodegeneration in Alzheimer's disease. *Nat Neurosci* **24**, 786-798,
1031 doi:10.1038/s41593-021-00851-3 (2021).
- 1032 53 Consortium, G. T. The GTEx Consortium atlas of genetic regulatory effects across human
1033 tissues. *Science* **369**, 1318-1330, doi:10.1126/science.aaz1776 (2020).
- 1034 54 Consortium, G. T. The Genotype-Tissue Expression (GTEx) project. *Nat Genet* **45**, 580-
1035 585, doi:10.1038/ng.2653 (2013).
- 1036 55 Li, G. *et al.* Extensive promoter-centered chromatin interactions provide a topological
1037 basis for transcription regulation. *Cell* **148**, 84-98, doi:10.1016/j.cell.2011.12.014 (2012).
- 1038 56 Diao, Y. *et al.* A tiling-deletion-based genetic screen for cis-regulatory element
1039 identification in mammalian cells. *Nat Methods* **14**, 629-635, doi:10.1038/nmeth.4264
1040 (2017).
- 1041 57 Uyehara, C. M. & Apostolou, E. 3D enhancer-promoter interactions and multi-connected
1042 hubs: Organizational principles and functional roles. *Cell Rep*, 112068,
1043 doi:10.1016/j.celrep.2023.112068 (2023).
- 1044 58 Miyaoka, Y. *et al.* Isolation of single-base genome-edited human iPS cells without
1045 antibiotic selection. *Nat Methods* **11**, 291-293, doi:10.1038/nmeth.2840 (2014).

- 1046 59 Cerbini, T. *et al.* Transcription activator-like effector nuclease (TALEN)-mediated CLYBL
1047 targeting enables enhanced transgene expression and one-step generation of dual
1048 reporter human induced pluripotent stem cell (iPSC) and neural stem cell (NSC) lines.
1049 *PLoS One* **10**, e0116032, doi:10.1371/journal.pone.0116032 (2015).
- 1050 60 Li, B., Chen, P. B. & Diao, Y. CRISPR-SE: a brute force search engine for CRISPR design.
1051 *NAR Genom Bioinform* **3**, lqab013, doi:10.1093/nargab/lqab013 (2021).
- 1052 61 Perez, A. R. *et al.* GuideScan software for improved single and paired CRISPR guide RNA
1053 design. *Nat Biotechnol* **35**, 347-349, doi:10.1038/nbt.3804 (2017).
- 1054 62 Li, H. & Durbin, R. Fast and accurate short read alignment with Burrows-Wheeler
1055 transform. *Bioinformatics* **25**, 1754-1760, doi:10.1093/bioinformatics/btp324 (2009).
- 1056 63 Ross-Innes, C. S. *et al.* Differential oestrogen receptor binding is associated with clinical
1057 outcome in breast cancer. *Nature* **481**, 389-393, doi:10.1038/nature10730 (2012).
- 1058 64 Love, M. I., Huber, W. & Anders, S. Moderated estimation of fold change and dispersion
1059 for RNA-seq data with DESeq2. *Genome Biol* **15**, 550, doi:10.1186/s13059-014-0550-8
1060 (2014).
- 1061 65 Juric, I. *et al.* MAPS: Model-based analysis of long-range chromatin interactions from
1062 PLAC-seq and HiChIP experiments. *PLoS Comput Biol* **15**, e1006982,
1063 doi:10.1371/journal.pcbi.1006982 (2019).
- 1064 66 Rosen, J. D. *et al.* HPRep: Quantifying Reproducibility in HiChIP and PLAC-Seq Datasets.
1065 *Curr Issues Mol Biol* **43**, 1156-1170, doi:10.3390/cimb43020082 (2021).
- 1066 67 Yu, G., Wang, L. G., Han, Y. & He, Q. Y. clusterProfiler: an R package for comparing
1067 biological themes among gene clusters. *OMICS* **16**, 284-287, doi:10.1089/omi.2011.0118
1068 (2012).
- 1069 68 Robinson, M. D., McCarthy, D. J. & Smyth, G. K. edgeR: a Bioconductor package for
1070 differential expression analysis of digital gene expression data. *Bioinformatics* **26**, 139-
1071 140, doi:10.1093/bioinformatics/btp616 (2010).
- 1072 69 Kubo, N. *et al.* Promoter-proximal CTCF binding promotes distal enhancer-dependent
1073 gene activation. *Nat Struct Mol Biol* **28**, 152-161, doi:10.1038/s41594-020-00539-5 (2021).
- 1074 70 Zhang, Y. *et al.* Model-based analysis of ChIP-Seq (MACS). *Genome Biol* **9**, R137,
1075 doi:10.1186/gb-2008-9-9-r137 (2008).
- 1076 71 Heinz, S. *et al.* Simple combinations of lineage-determining transcription factors prime cis-
1077 regulatory elements required for macrophage and B cell identities. *Mol Cell* **38**, 576-589,
1078 doi:10.1016/j.molcel.2010.05.004 (2010).
- 1079 72 Li, Y. *et al.* DeepGWAS: Enhance GWAS Signals for Neuropsychiatric Disorders via Deep
1080 Neural Network. *Res Sq*, doi:10.21203/rs.3.rs-2399024/v1 (2023).
- 1081 73 Huang, L. *et al.* TOP-LD: A tool to explore linkage disequilibrium with TOPMed whole-
1082 genome sequence data. *Am J Hum Genet* **109**, 1175-1181,
1083 doi:10.1016/j.ajhg.2022.04.006 (2022).
- 1084 74 Anzalone, A. V. *et al.* Search-and-replace genome editing without double-strand breaks
1085 or donor DNA. *Nature* **576**, 149-157, doi:10.1038/s41586-019-1711-4 (2019).
- 1086 75 Hsu, J. Y. *et al.* PrimeDesign software for rapid and simplified design of prime editing
1087 guide RNAs. *Nat Commun* **12**, 1034, doi:10.1038/s41467-021-21337-7 (2021).
- 1088

Figure 1

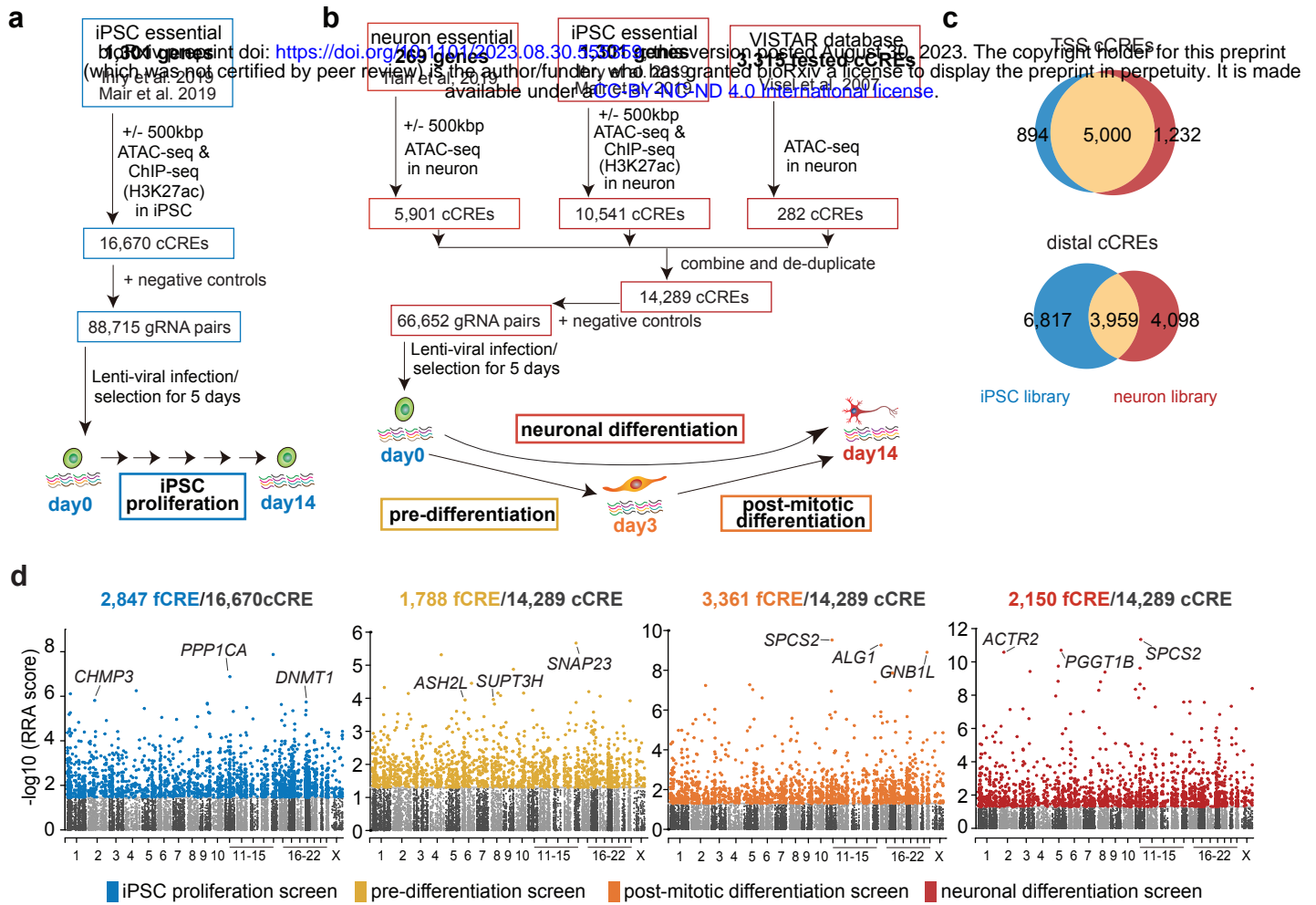


Figure 2

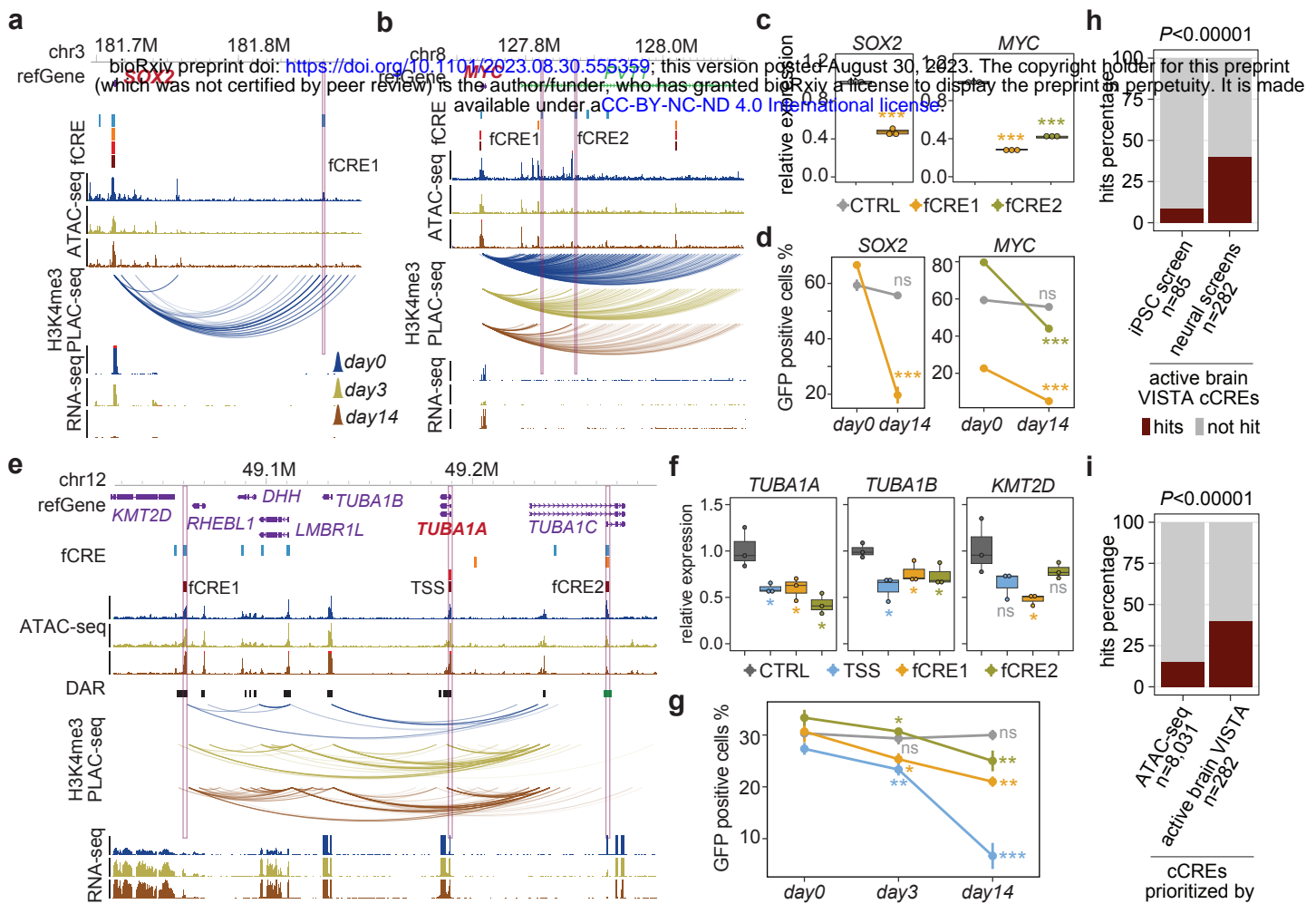


Figure 3

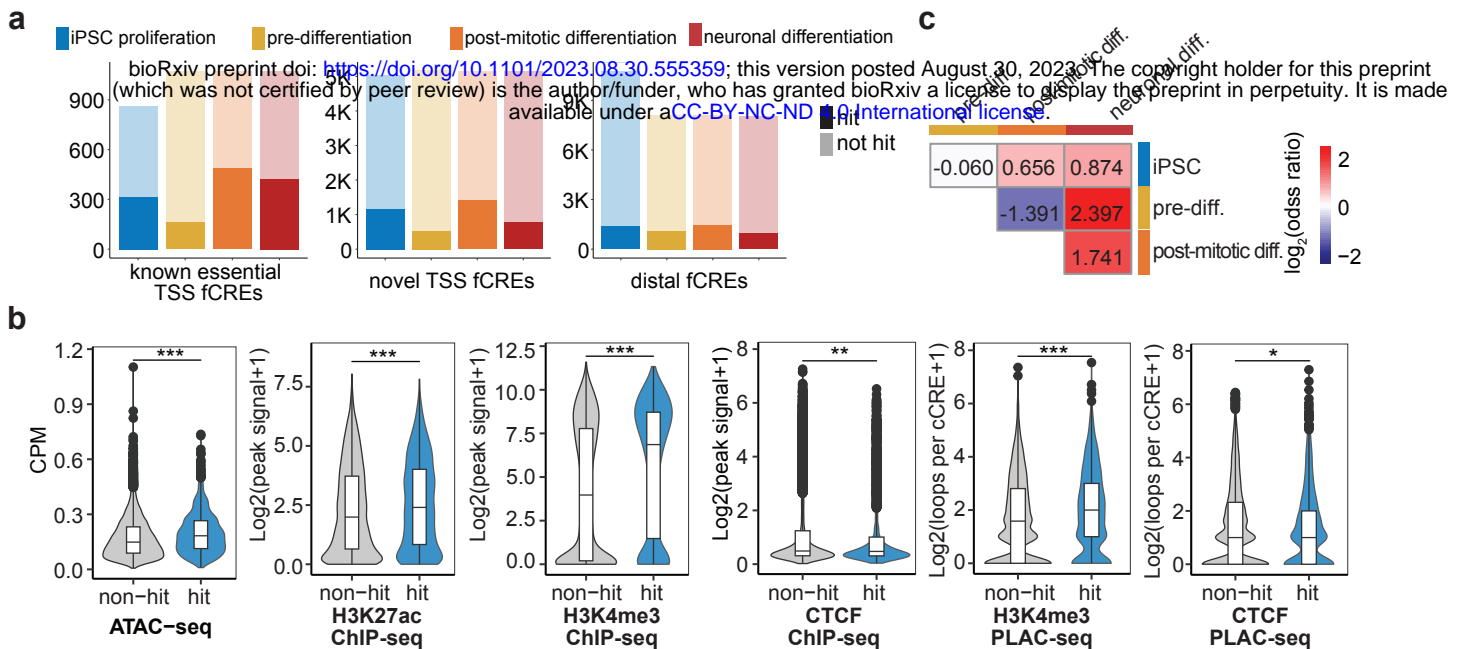


Figure 4

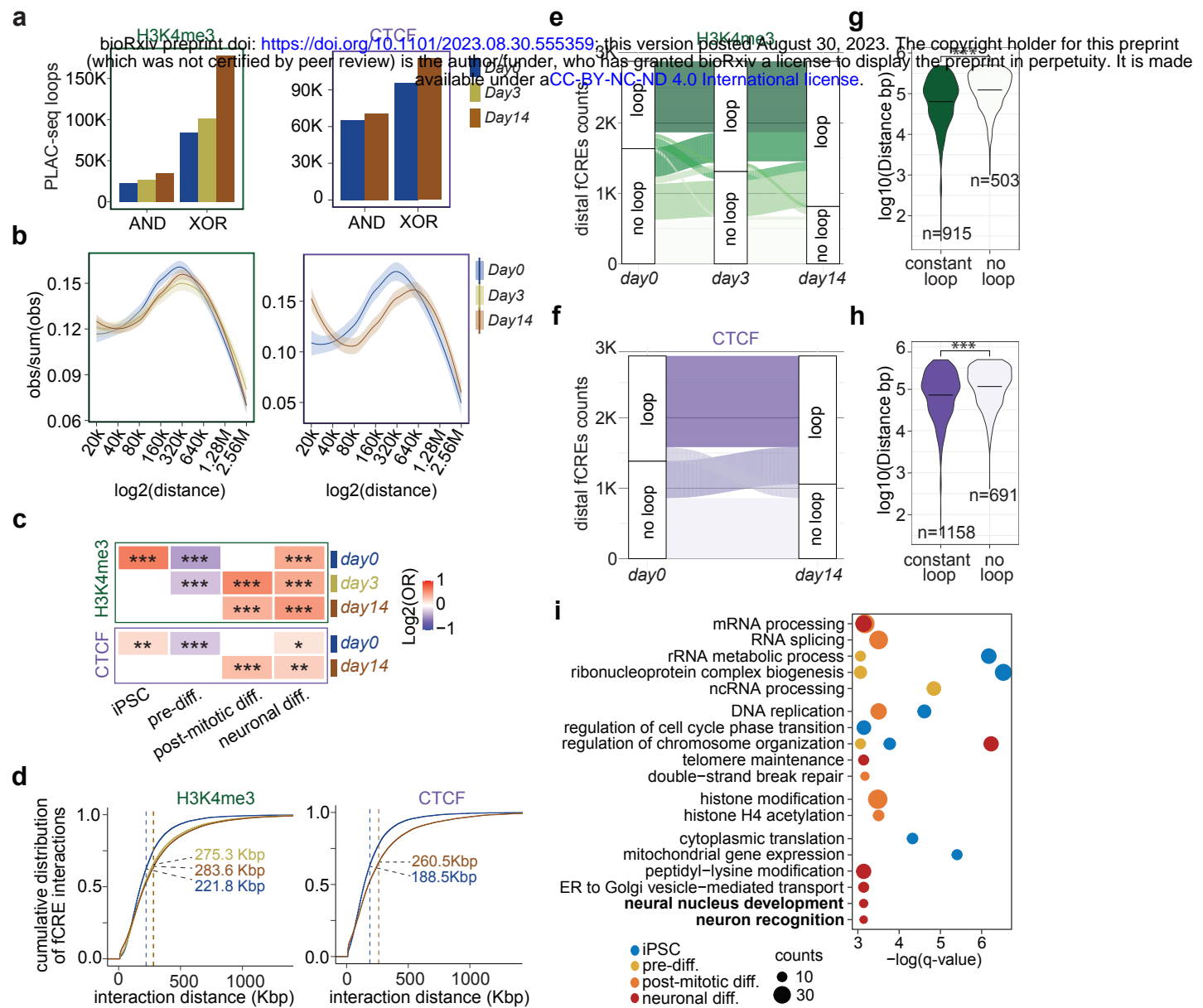


Figure 5

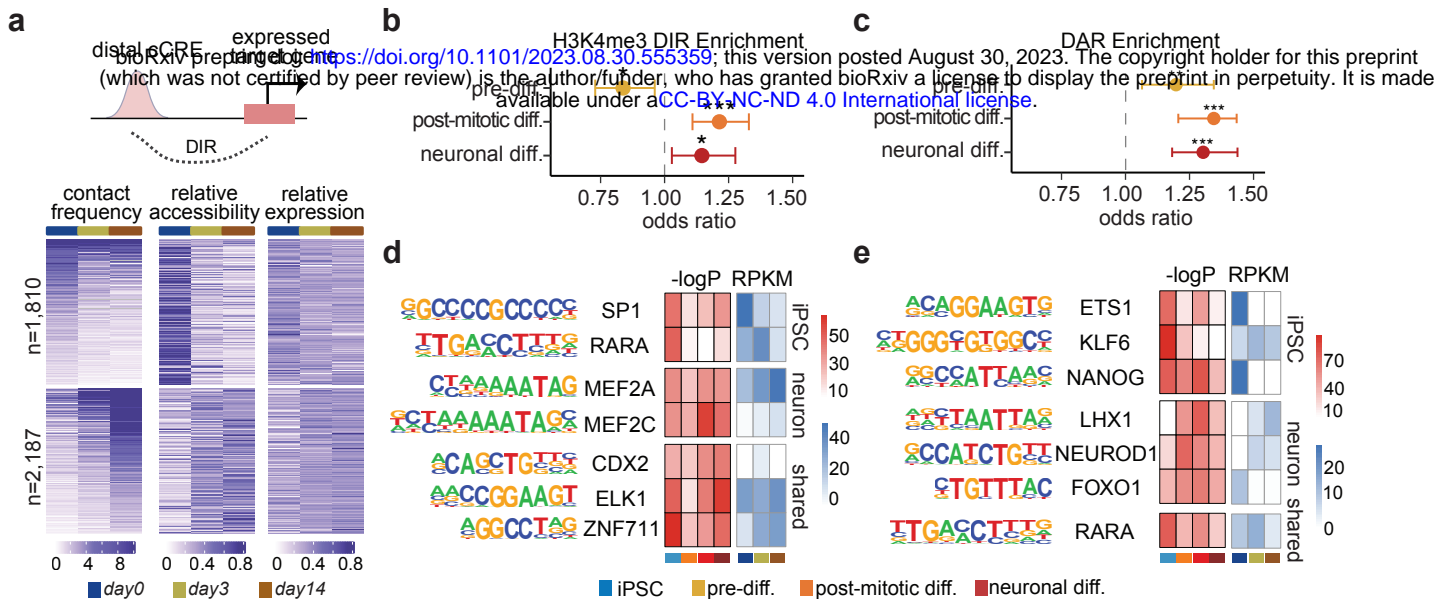
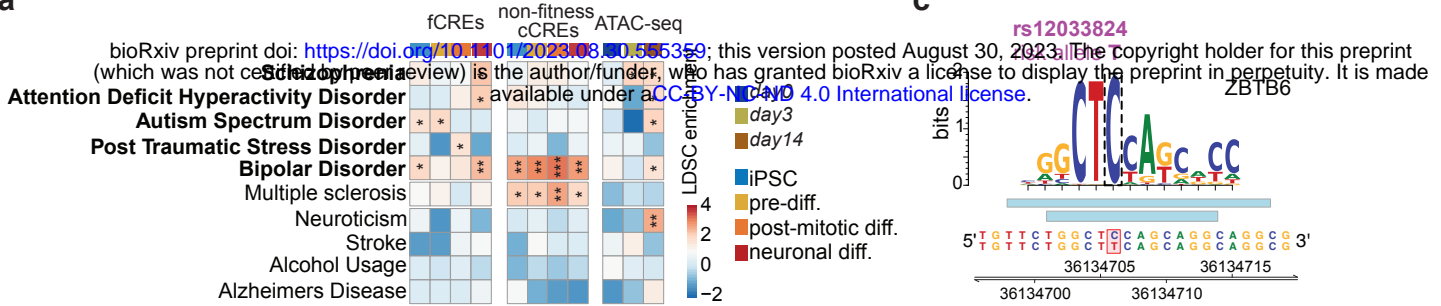
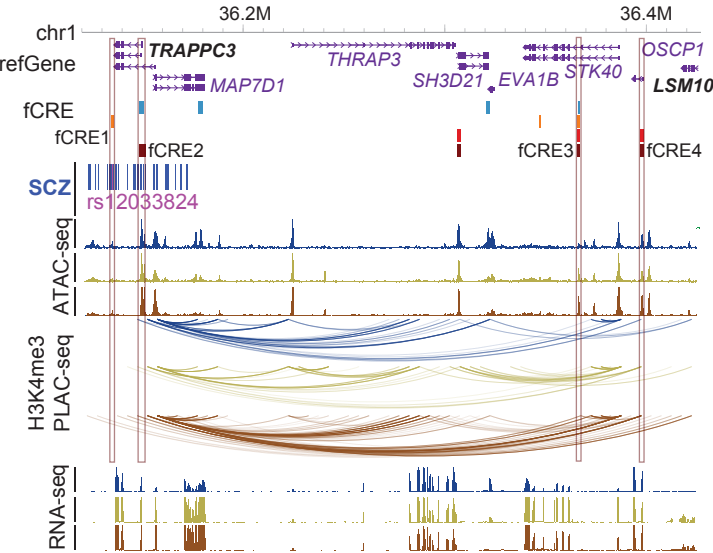


Figure 6

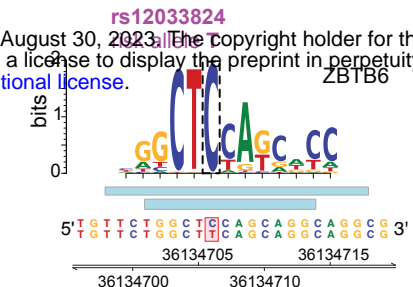
a



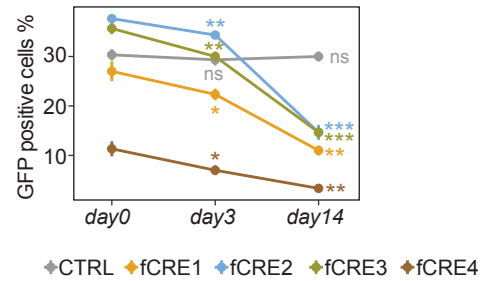
b



c



d



e

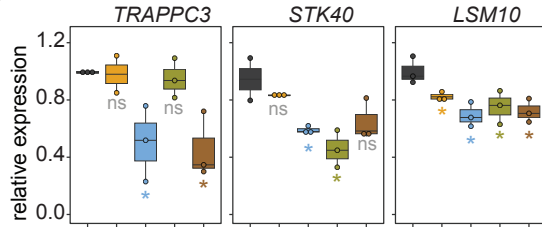
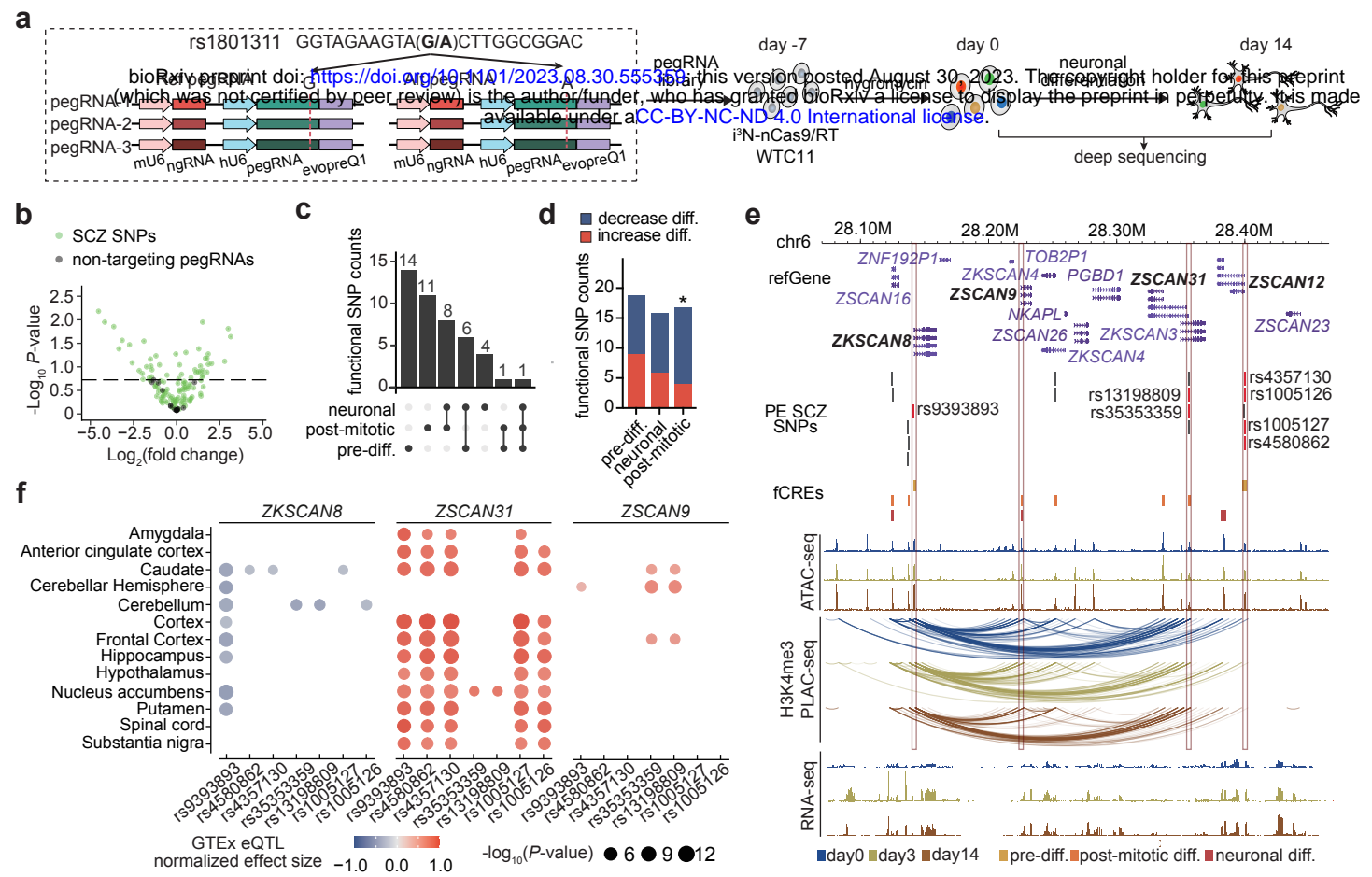
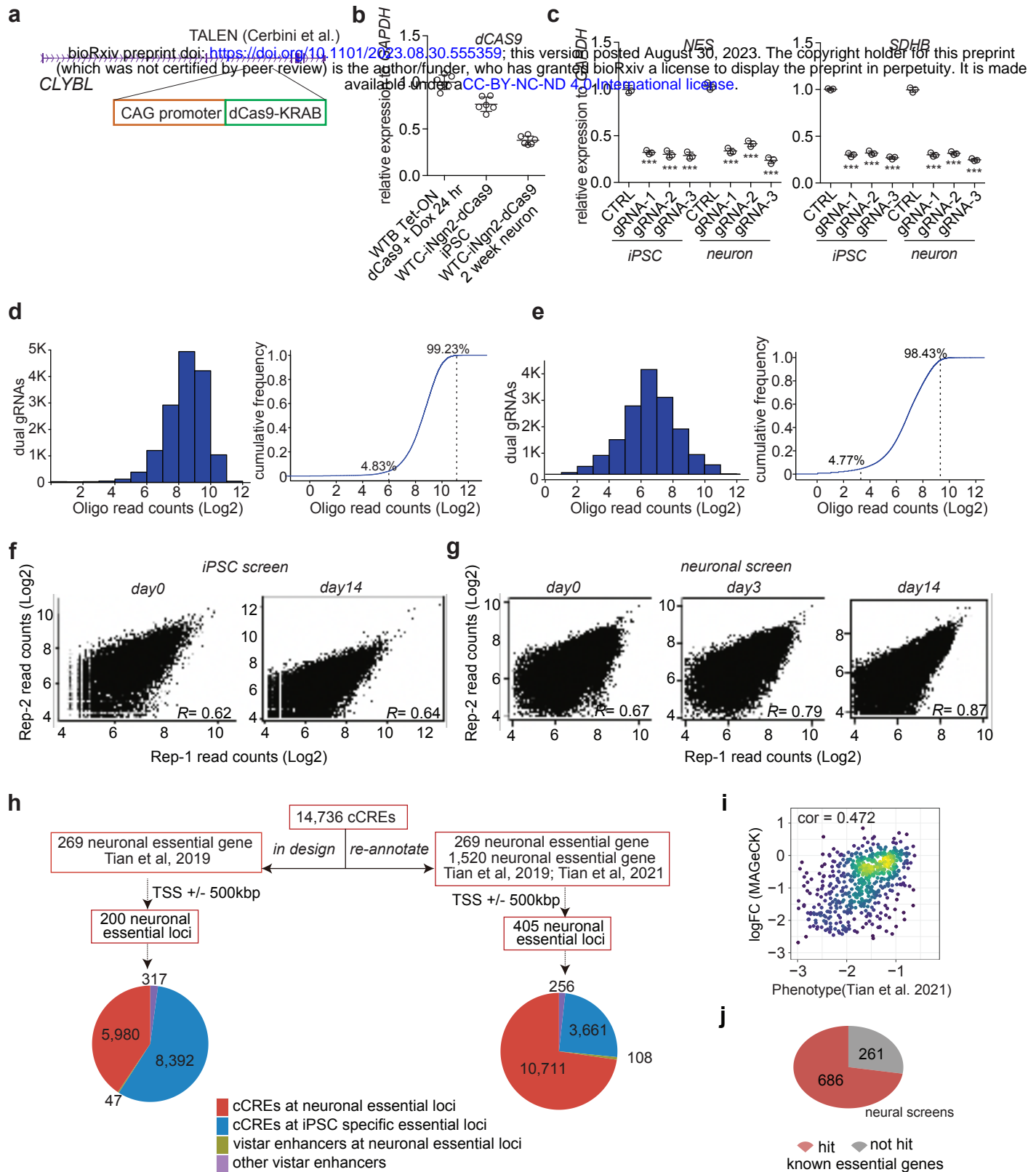


Figure 7

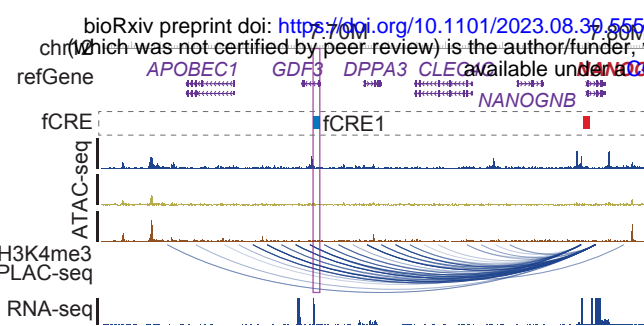


Extended Data Figure 1

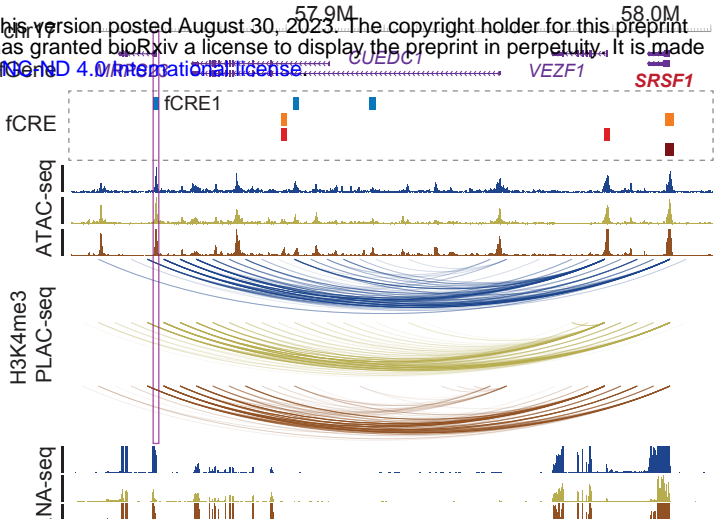


Extended Data Figure 2

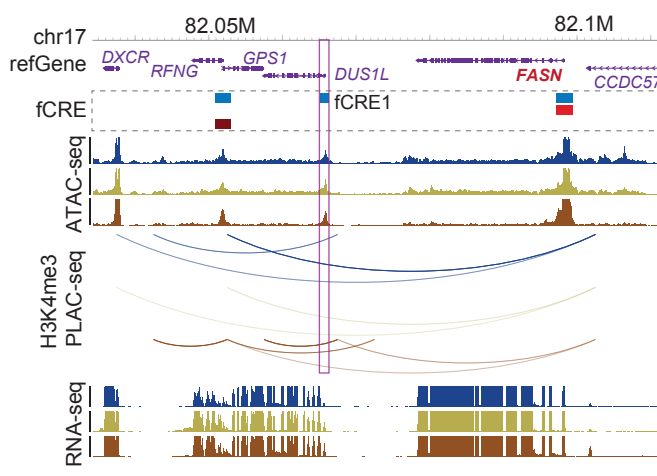
a



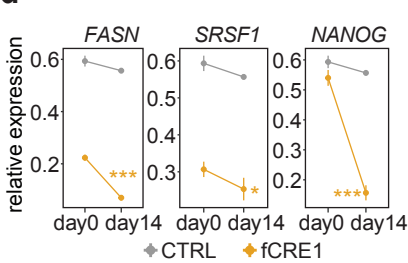
b



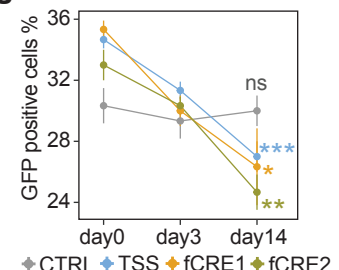
c



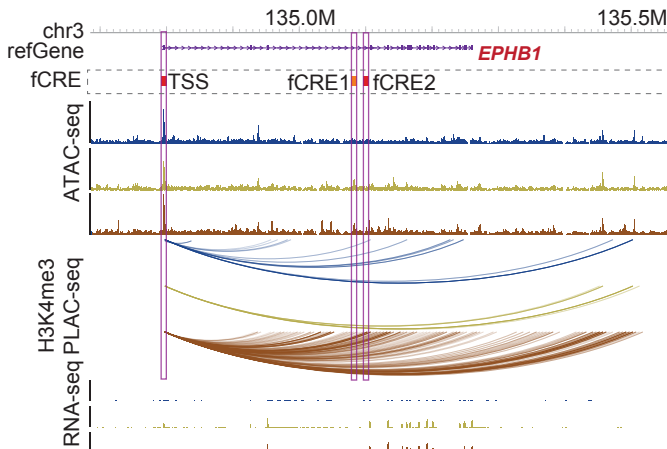
d



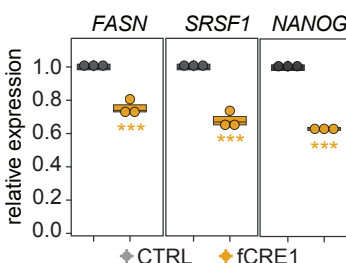
g



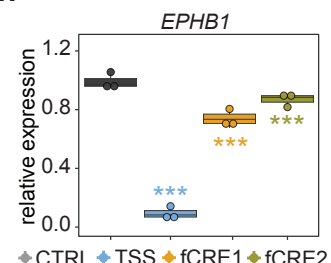
f



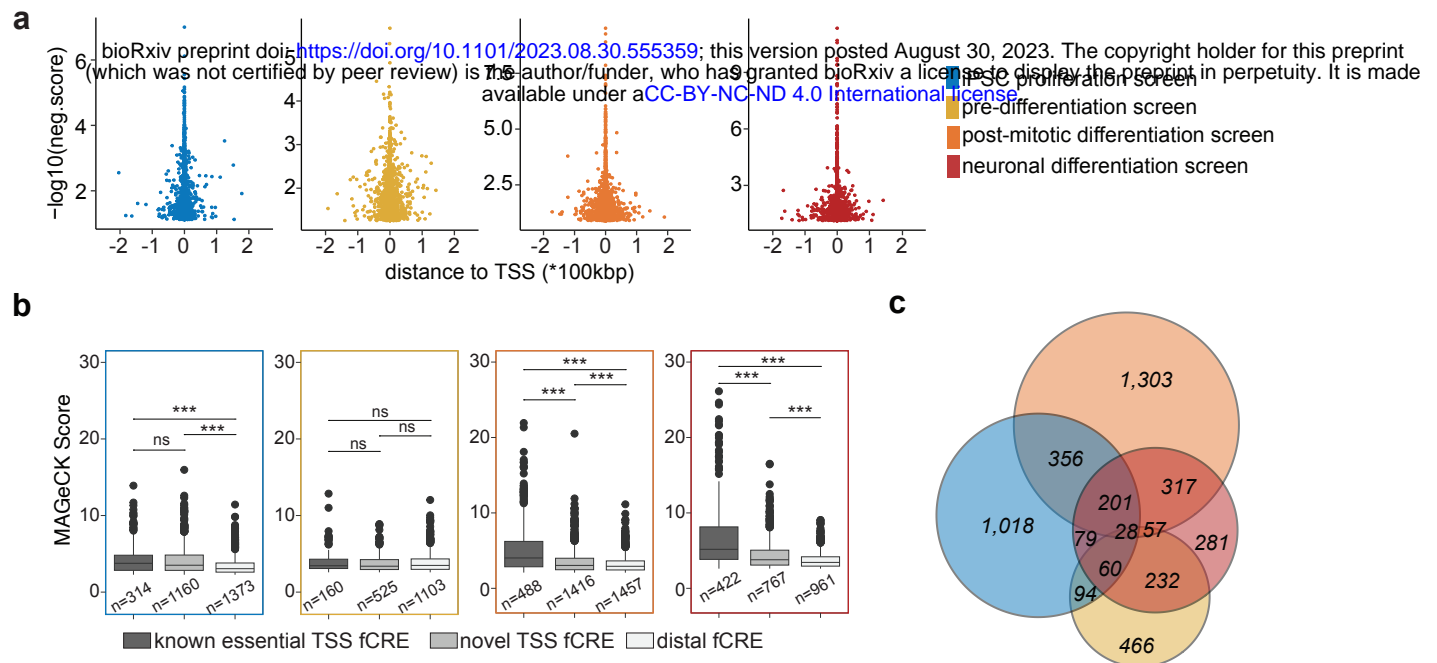
e



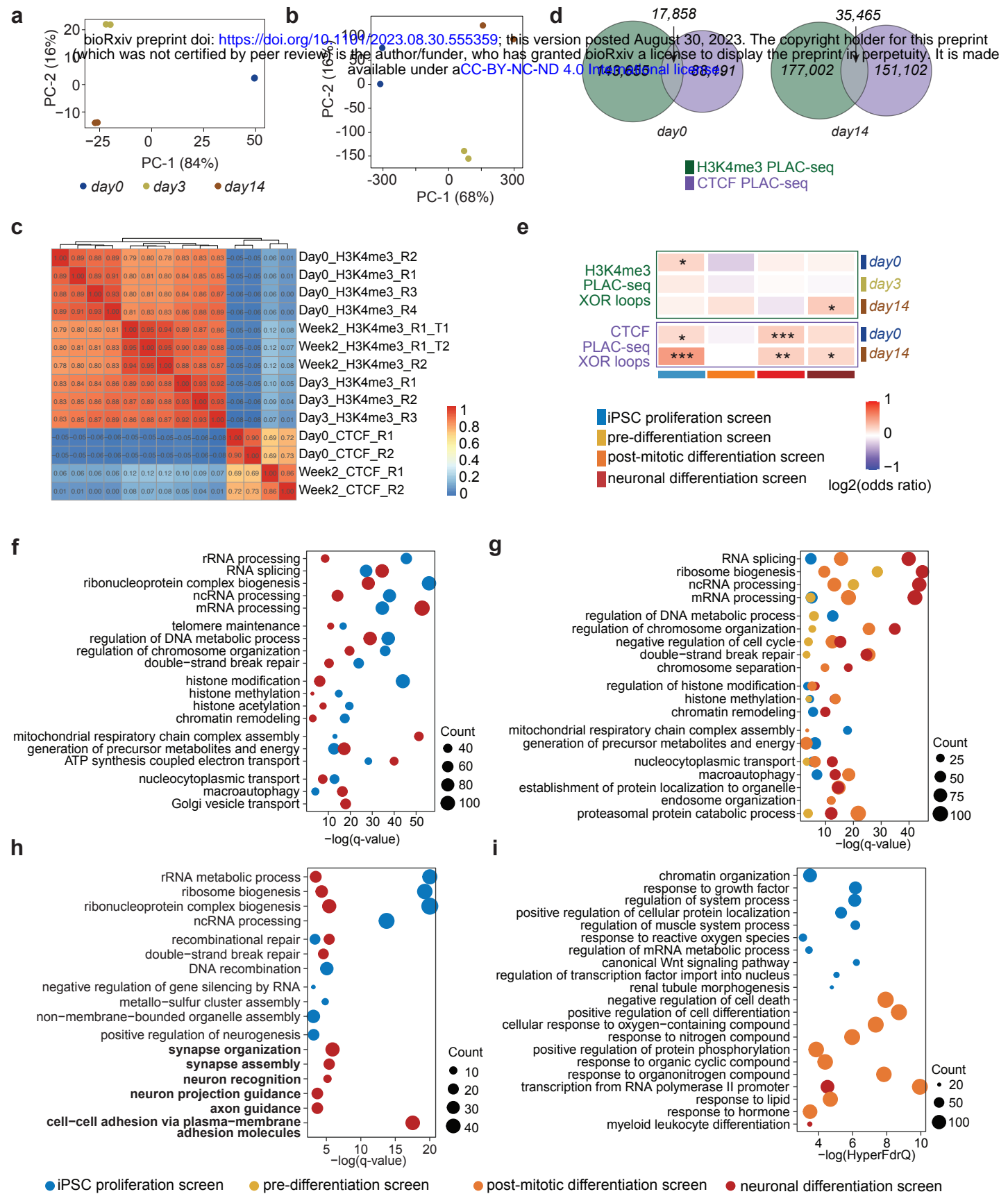
h



Extended Data Figure 3

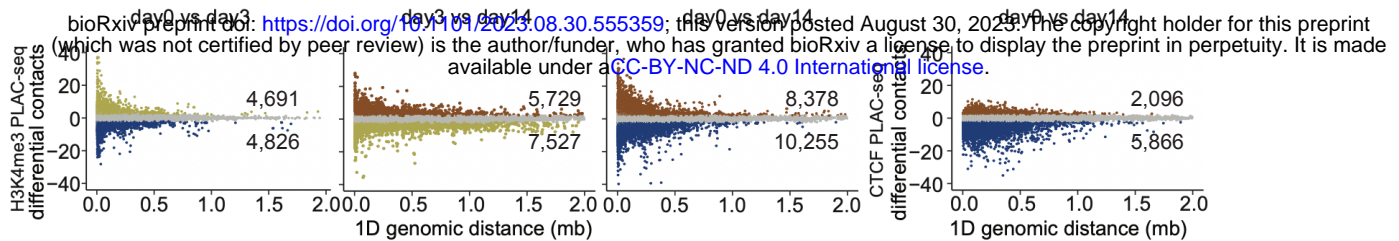


Extended Data Figure 4

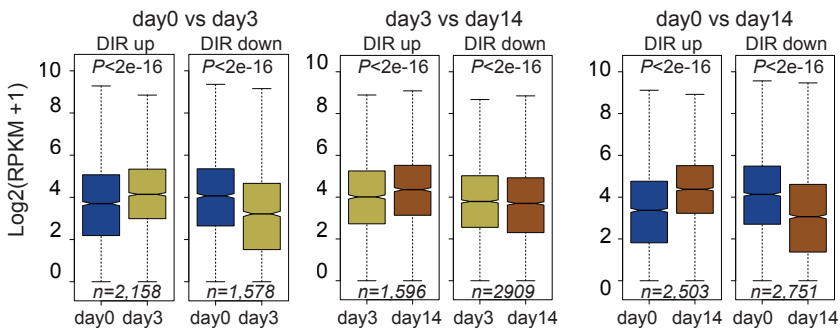


Extended Data Figure 5

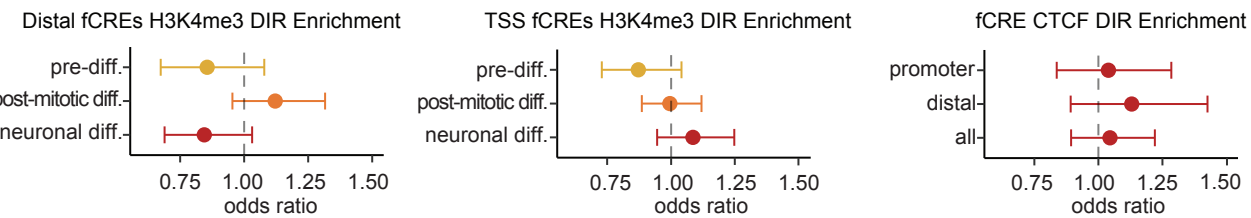
a



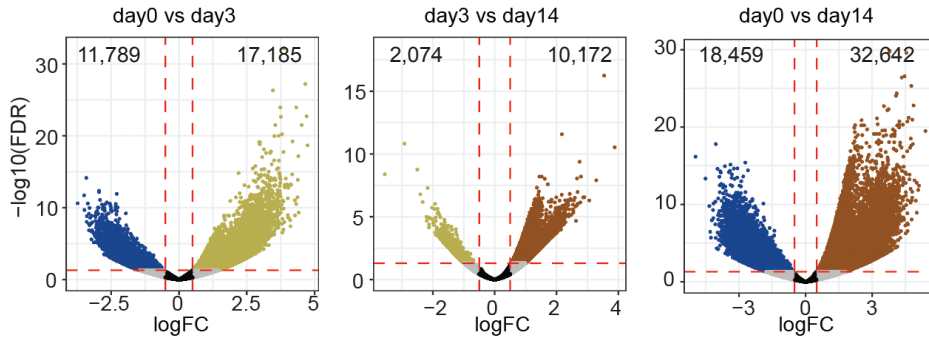
b



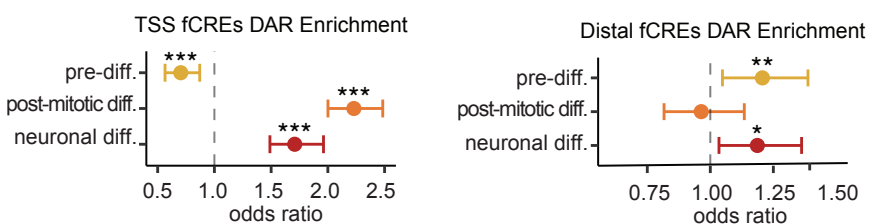
c



e

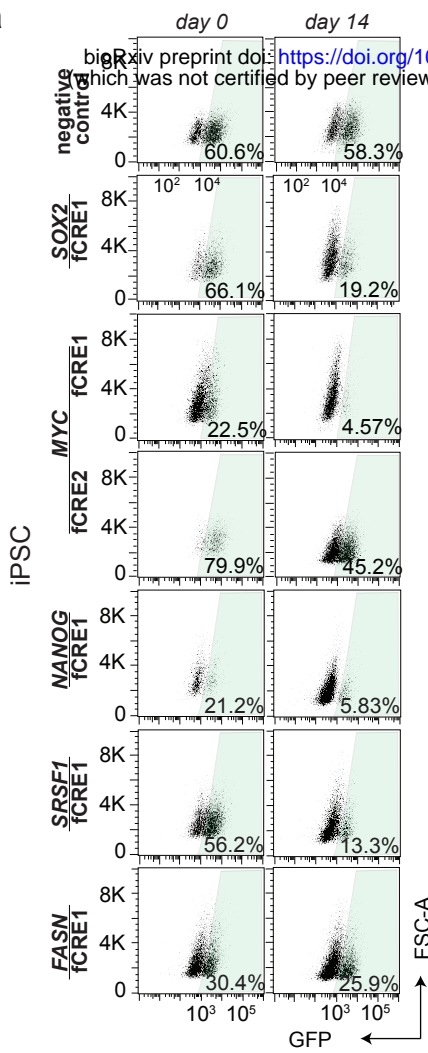


f

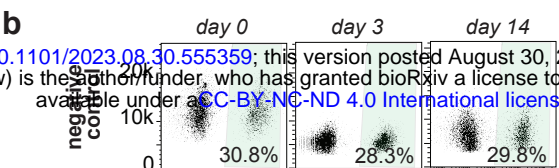


Extended Data Figure 6

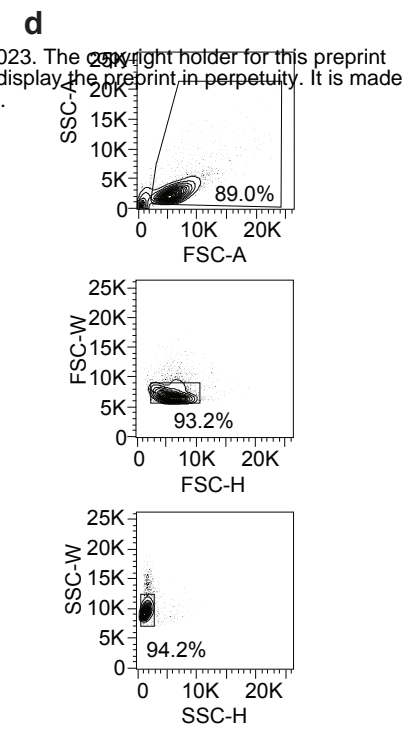
a



b



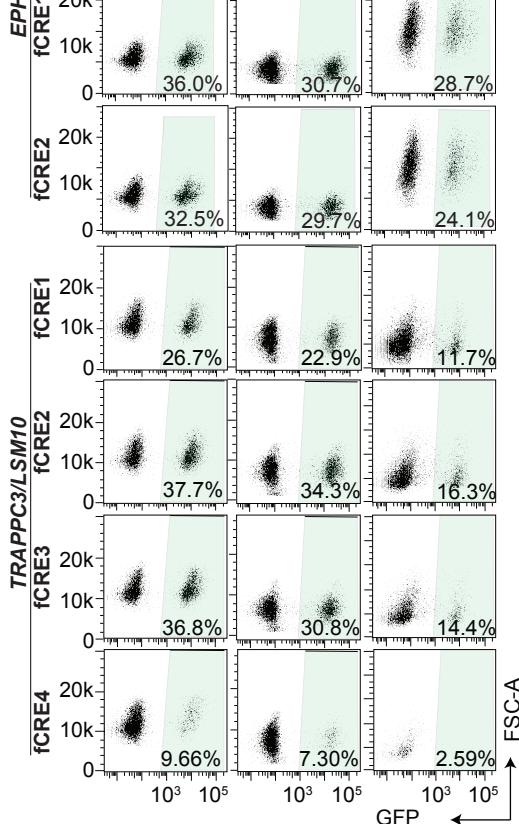
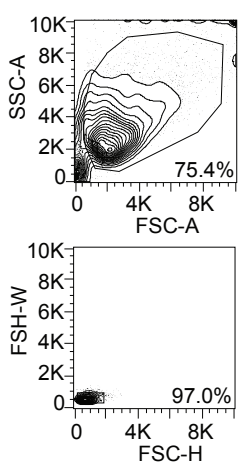
d



iPSC

neuron

c



Extended Data Figure 7

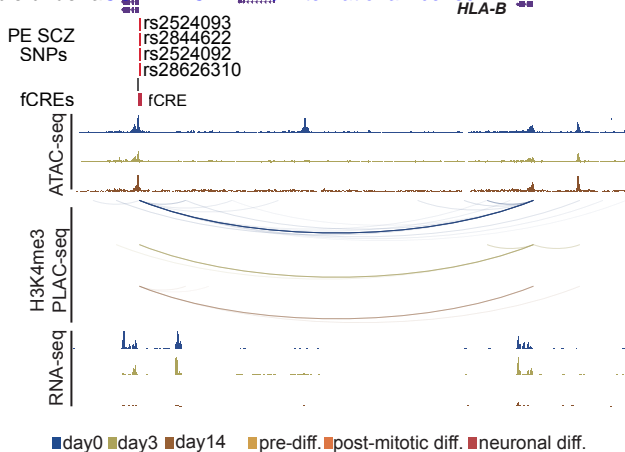
a

TALEN (Cerbini et al.)
 bioRxiv preprint doi: <https://doi.org/10.1101/2023.08.30.555359>; this version posted August 30, 2023. The copyright holder for this preprint (which was not certified by peer review) is the author/funder, who has granted bioRxiv a license to display the preprint in perpetuity. It is made available under aCC-BY-NC-ND 4.0 International license.

CLYBL



c



b

